



State of Science on Emission Rate Thresholds for Upstream Petroleum Industry Leaks Corresponding to a Range of ppm Concentration Based Thresholds

Prepared for:

Petroleum Technology Alliance Canada Suite 400, Chevron Plaza 500 – Fifth Avenue S.W. Calgary, Alberta T2P 3L5

and

Clean Resource Innovation Network The Energy Transition Centre 112 4th Avenue SW, Suite 1500 Calgary, AB T2P 0H3

Prepared by:

Equilibrium Environmental Inc. 3004 Ogden Road SE Calgary, Alberta T2G 4N5

Tel: (403) 286-7706 Fax: (403) 286-8173

www.eqm.ca

Email: <u>tknafla@eqm.ca</u>

msommers@eqm.ca

Project Number: PT-20; CR-02 Date of Submission: June 2024

TABLE OF CONTENTS

		Page					
1 INTR	RODUCTION AND WORK SCOPE	1					
1.1	Introduction	1					
1.2							
2 FEDI	ERAL AND PROVINCIAL GUIDELINES	2					
3 MET	HANE DETECTION TECHNOLOGY	3					
3.1	Calorimetric Sensors	3					
3.2	Flame Ionization Detector (FID)	4					
3.3	Photoionization Detector (PID)						
3.4	Infrared (IR)	5					
3.5	Laser Spectroscopy	7					
3.6	High Flow Sampler (HFS) Detection	8					
3.7	Optical Gas Imaging (OGI)	10					
3.8							
3.9	LiDAR Sensors	15					
4 PPM	IV AND CFM REGRESSION ANALYSIS	17					
4.1	Mass Emission Correlation Equations	17					
4.2	Dataset Analysis						
	Sage Dataset	19					
	HNOLOGY DISCUSSION						
5.1	Third Party Methods Evaluation						
	1.1 Concawe European Field Studies						
5.2	Alberta Methane Field Challenge	27					
5.3	METEC Evaluation of Dual Frequency Comb Spectroscopy	29					
6 REC	OMMENDATIONS FOR THE OIL AND GAS SECTOR	30					
6.1	Emissions Reporting Background	30					
6.2	Federal Taxation Background	34					
6.3	Summary and Recommendations						
7 CLO	SURE	38					
8 REF	FRENCES	39					

1 INTRODUCTION AND WORK SCOPE

1.1 INTRODUCTION

Methane (CH₄) is a colourless, odourless, and flammable Greenhouse Gas (GHG) that can be released into the atmosphere during exploration, extraction, production, and distribution of natural gas. The International Panel on Climate Change (IPCC) indicated in 2021 that approximately 60% of global CH₄ emissions originate from anthropogenic sources, and approximately 82.5 megatonnes (Mt) can be attributed to oil and gas activity. Fugitive CH₄ accounted for 8.2% of total emissions in Canada in 2021 (Environment and Climate Change Canada (ECCC), 2023a). Despite having a shorter atmospheric lifespan than carbon dioxide (CO₂), CH₄ absorbs more energy making it 28-36x more potent than CO₂ as a GHG over a 100-year period.

The IPCC estimated that in 2021, 180 billion cubic meters of gas have leaked globally during oil and gas operations. Leaks can be unplanned events as well as intentional due to specific required maintenance procedures associated with equipment design, such as pneumatic valve controllers. In Canada, 13% of the nation's total GHG emissions are due to CH₄, and of this, approximately 40% is sourced from the oil and gas sector (ECCC, 2021).

To reduce contributions to GHG emissions, the Leak Detection and Repair (LDAR) initiative has become a regulated (ECCC with provincial equivalency agreements) industry standard in Canada. Emissions associated with leaks must be reported in addition to regular annual disclosure of GHG emissions from typical oil and gas industrial operations that are not associated with leaks. Emission rates are reported on a tonnes/year basis, which is a mass flow rate metric. Requiring emissions to be reported using this metric creates challenges for LDAR programs based on a part per million volume-based metric (a concentration metric).

The LDAR compliance threshold is defined by ECCC as 500 ppmv – leaks detected at higher concentrations are flagged for mitigative action. Methods have been developed to measure fugitive volatile organic compounds (VOCs) as well as CH₄ concentrations. The United States Environmental Protection Agency (US EPA) developed Method 21 (US EPA, 2017) for measuring VOC and CH₄ concentrations. Various measurement instruments are available for assessing compliance, as laid out in Method 21. ECCC (2018a) similarly lists eligible leak detection instruments, primarily referencing the Method 21 document.

GHG emission inventories can be determined based on equipment component counts, fluid throughput, and estimates of component-specific leakage rates and probability (Jamin, 2018). Average emission factor (EF) values can be applied (such as those summarized by US EPA, 1995) to derive mass emission leak rates for GHG reporting, albeit with considerable uncertainty and lack of accuracy.

While ppmv measurements are of considerable value for an LDAR program as compliance is measured against a ppmv threshold, they have limited value for reporting GHG mass emissions under section 46 of the *Canadian Environmental Protection Act* (CEPA) (ECCC, 1999), which requires a tonnes/yr metric. Correlations are available, such as those provided by US EPA (1995),

for estimating mass emission rates from ppmv data for GHG reporting. These correlations can be infrastructure component (e.g., valve, flange) and VOC type specific, leading to greater refinement, and were primarily focused on VOCs rather than CH₄.

While correlations that are component and VOC type specific may have improved accuracy over the use of EFs and equipment counts for estimating mass emission rates, they do not reflect variability in mass emission rates due to differences in equipment status, meteorological conditions, operating environment, and numerous other factors. As a result, the use of correlations is associated with uncertainty when LDAR data on a ppmv basis are used to quantify leak-related GHG emission rates. For example, the California Air Resources Board (Sage, 2019) citing regression work summarized by the US EPA (1995), indicated r^2 values for regressions specific to equipment types such as valves and flanges of 0.609 and 0.753, respectively. While a $r^2 > 0.7$ can be considered a good correlation, it is associated with considerable variability in quantifying emissions on a mass emission rate basis extrapolated from a ppmv measurement.

More recently, technological advances have improved detection limits and accuracy of equipment that measures mass emission rates of CH₄, which has the potential to improve the quality of GHG emission inventories as well as the implementation of LDAR programs. This in part requires a LDAR threshold expressed on a mass emission (or flow rate) basis, which can be considered comparable to the federal threshold of 500 ppmv or provincial threshold of 10,000 ppmv.

1.2 SCOPE OF WORK

The scope of this report includes an overview of federal and provincial guidelines, an overview of detection sensors and devices currently on the market, discussion on regression models that can convert ppmv to a mass emission or flow rate measurement, and recommendations on steps forward to optimize emission regulation using flow rate measurement equipment.

2 FEDERAL AND PROVINCIAL GUIDELINES

Effective January 1, 2020, Environment and Climate Change Canada (ECCC) mandated in SOR_2018-66 § 3.4 that CH₄ leaks must be detected with an approved Method 21 instrument (US EPA, 2017) or optical gas imaging technology with a resolution capable of detecting 250 ppmv of CH₄, or a flow rate of 60 grams per hour (g/hr). If an industrial component (e.g., connector, pump, valve) is measured to be leaking CH₄ with a concentration of 500 ppmv or greater, it must be repaired within 30 days or during the next planned shutdown, provided the cumulative site-specific emission volume is less than the environmental impact emission volume of taking corrective action within a 30-day repair window.

In contrast, the Alberta Energy Regulator's (AER) guidance presented in Directive 060 § 8.10.4 stipulates the measurement instrument must detect a CH₄ concentration of 500 ppmv operated in accordance with Method 21 (EPA, 2017), or a gas-imaging camera capable of detecting pure CH₄ at a flow rate of 1.0 gram per hour under lab conditions. Measured leaks less than 10,000

ppmv do not need to be repaired within 30 days, but the emission must be quantified at subsequent surveys until a repair is completed.

An equivalency agreement was set in 2020 between the province and federal government (Agreement on the Equivalency of Federal and Alberta Regulations Respecting the Release of Methane from the Oil and Gas Sector in Alberta, 2020) as well as the equivalent provisions under the Methane Emission Reduction Regulation, A.R. 244/2018 (MERR) struck in Alberta, which are legally binding. The federal ECCC CH₄ regulation also defines limits on the venting of gas from pneumatic pumps and controllers that vent gas as part of normal mechanical operation. This has relevance for Class V valves that similarly vent as a consequence of safe operation requirements and mechanical design.

3 METHANE DETECTION TECHNOLOGY

A wide array of methane detection devices is available on the market today that differ by sensor type, accuracy, portability, unmanned continual surveillance or ability to capture flow rate.

3.1 CALORIMETRIC SENSORS

Calorimetric sensors used for methane detection are typically found in portable, point source devices such as the RKI EAGLE 2 or Hetek Flow Sampler. Typically, there are three components that comprise a calorimetric sensor device: a temperature sensor, catalytic combustor and heater device. An exothermic reaction occurs when methane oxidizes when in contact with heated rareearth elements such as platinum, palladium, or rhodium catalysts thereby releasing additional heat, which is converted to a sensing signal (Figure 1; Aldhafeeri et al., 2020). Accuracy can range from +/- 50 parts per million (ppm) to 5% of the screen value (SV) or device reading with an upper limit of 50,000 ppm. Calorimetric sensors are low cost and simple designs, however, they are less optimal for lower concentrations.

(physico-) electrical physical chemical signal: measurand: data interaction voltage heat calorimetric recording transducer and processing sensitive layer

Figure 1. Calorimetric Gas Detection Process

Source: Aldhafeeri, et al. (2020).

3.2 FLAME IONIZATION DETECTOR (FID)

FID sensors typically use hydrogen-air flame and two electrodes connected to a battery in portable, point source devices such as the Thermo Scientific TVA-1000B, TVA2020 or LDAR Tools PHX42. The sample is fed into a hydrogen flame that via combustion, ionizes particles if the sample contains compounds with carbon and hydrogen. The ions increase the electrical current flow between electrodes, which is measured at the electrode sensor and is proportion to the mass of hydrocarbons (Figure 2). FIDs are very sensitive to detection and extremely accurate. However, the sample is non-recoverable and cannot be used for any additional analysis. Accuracy can range from +/- 0.5 ppm up to +/- 10 % of SV with an upper limit of 50,000 ppm. Fewer FID devices remain on the market as the necessity for hydrogen fuel and refill systems has become a deterrent to their common use in the field.

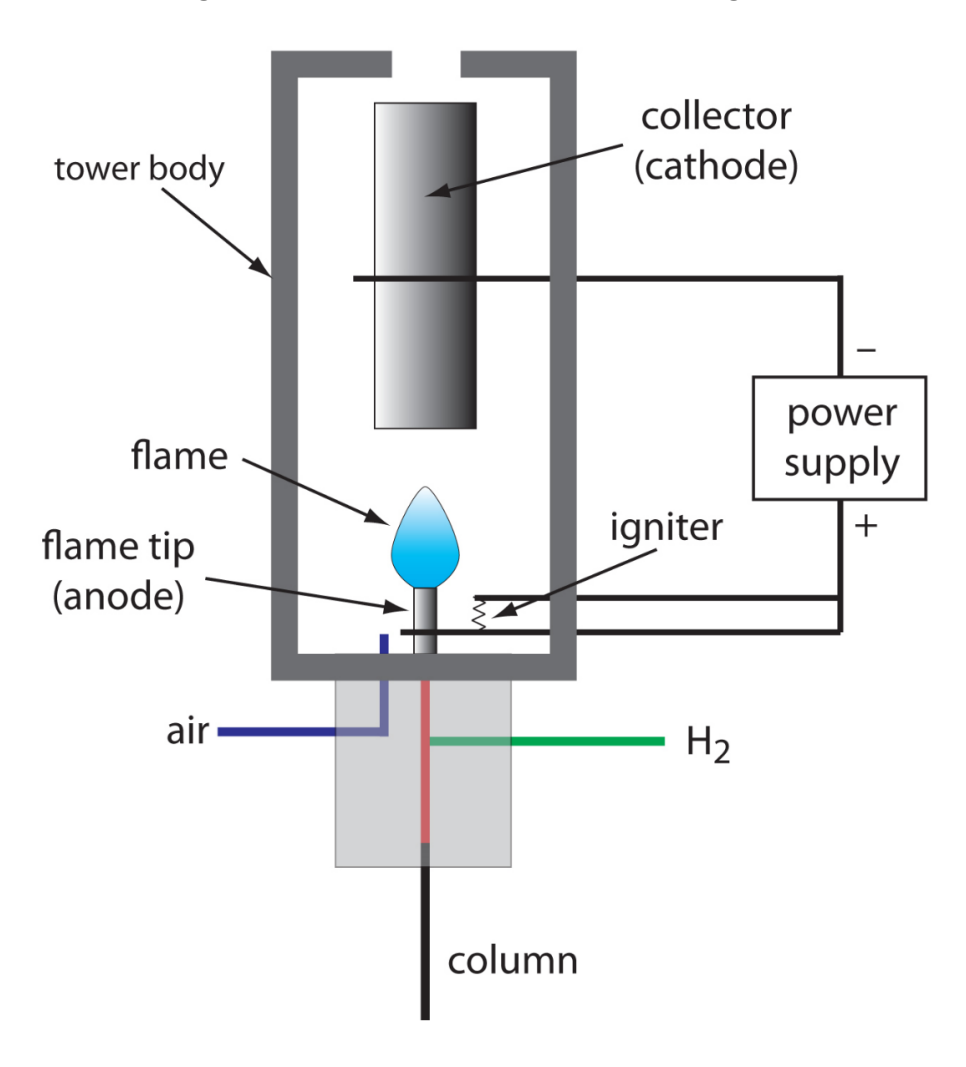


Figure 2. Flame Ionization Detection Diagram

Source: Harvey (2021). H₂ – Hydrogen gas; air – air sample used for methane detection.

3.3 PHOTOIONIZATION DETECTOR (PID)

PID sensors use ultraviolet (UV) light to ionize a sample, which occurs when the sample absorbs UV light and once ionized, negatively and positively charged ions are separated via charged plates. A current is measured that is proportional to the number of ions passing across the plates. (Figure 3). Typically PIDs used in the field cannot detect methane as the instruments are often setup with PID lamps with 10.6 or 11.7 eV bulbs whereas the ionization potential of methane is 12.61 eV. A surrogate approach can potentially be used for detecting CH₄ (RAE, 2014). PIDs are found in portable, point source devices such as the Thermo Scientific TVA-100-B or TVA2020, which also have an FID.

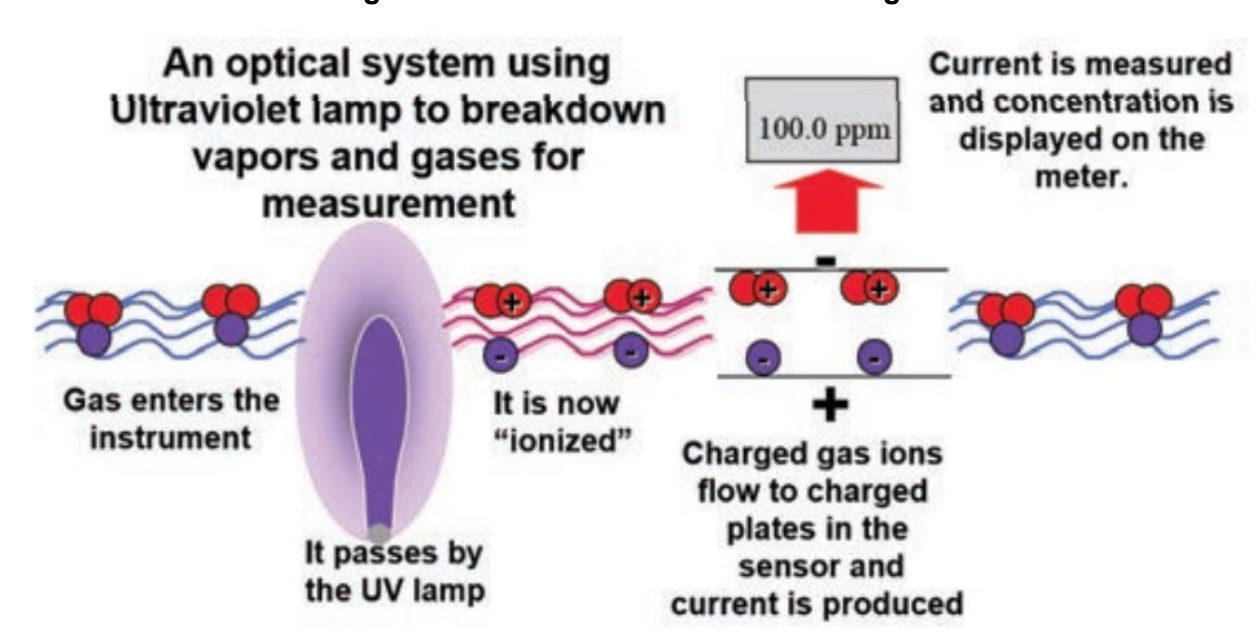


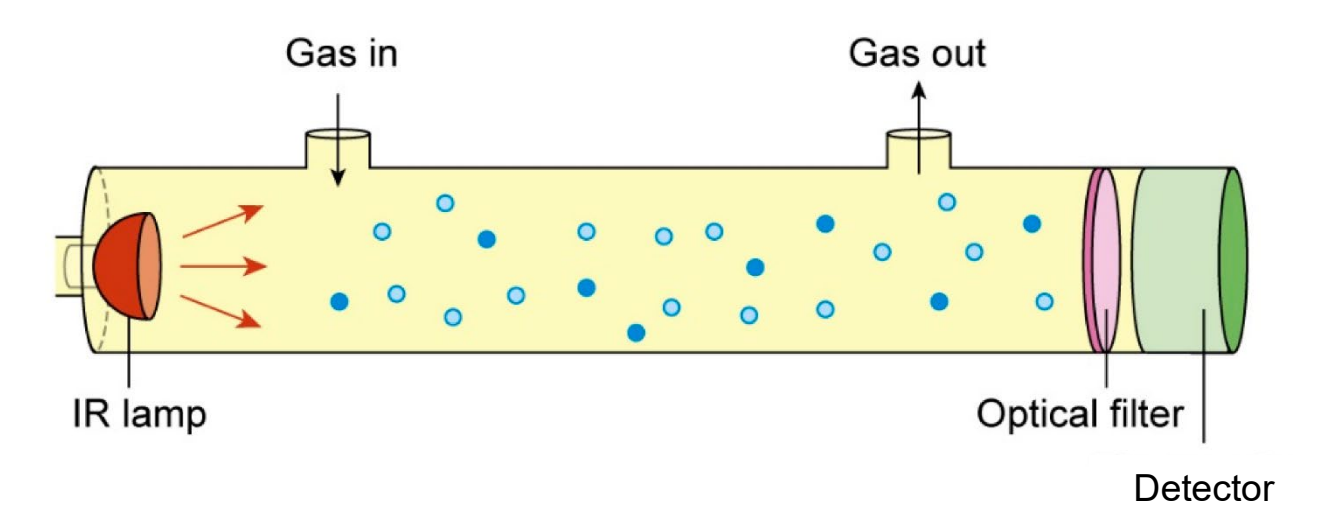
Figure 3. Photoionization Detection Diagram

Source: RAE (in press). UV - ultraviolet.

3.4 INFRARED (IR)

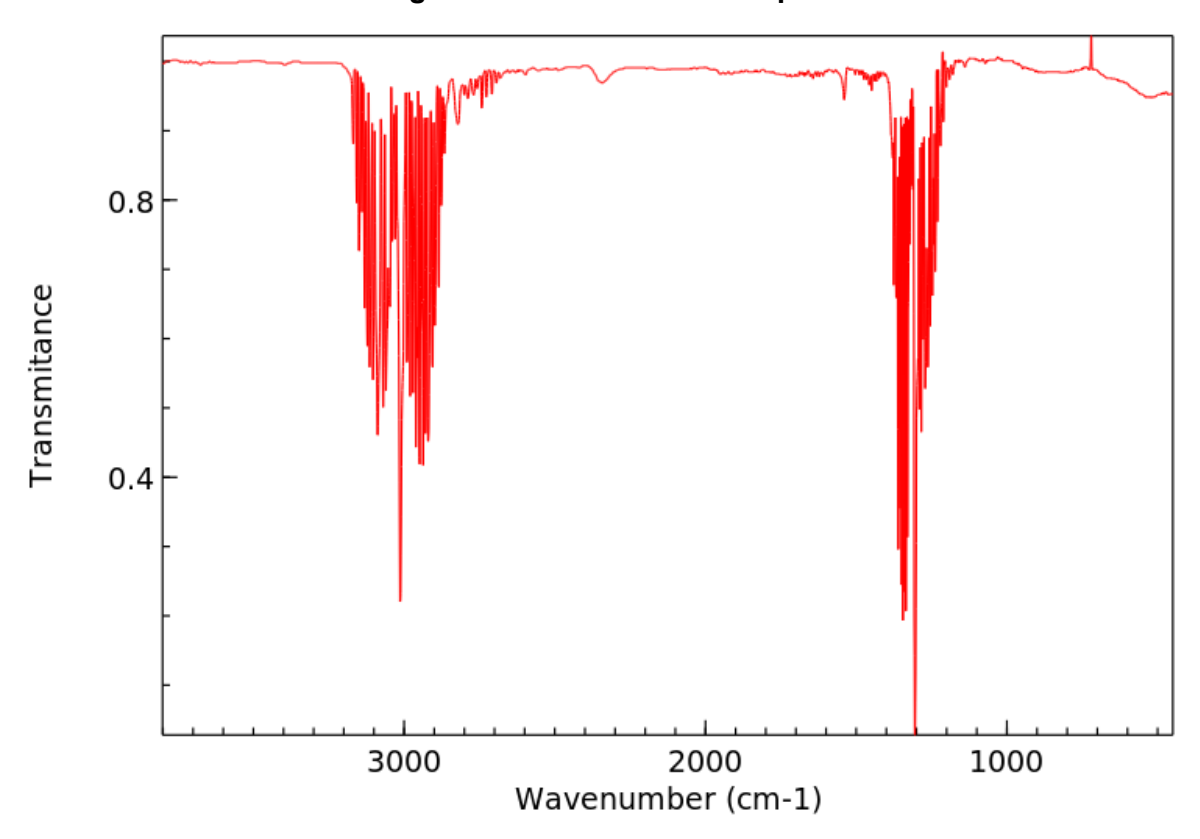
IR sensors used for CH₄ detection are found in numerous applications such as portable, point and area devices like ATO Gas CH4, Heath DP-IR+, Inficon Irwin, and RKI GX600, and fixed continuous devices such as MSA IR4500, MSA Ultima OPIR-5 (fixed devices come in ambient detection or open-path detection). Accuracy ranges from +/- <3% to +/- 10% of the SV with an upper limit of 100%. IR CH₄ detection operates on the principle that CH₄ gas will absorb IR light at specific wavelengths tuned by an optical absorption filter. The measured variable filtered light is analyzed by a detector which determines the concentration of CH₄ gas (Figure 4). Methane has an absorption waveband of 3.07-3.71 μ m (Kang et al., 2022; Figure 6). Limitations of this technique includes the fact that gases such as ethane and propane absorb IR energy within this waveband range and cannot be differentiated from CH₄ (Taylor et al. 2008).

Figure 5. Infrared Detection Diagram



Source: Modified from Mendes et al. (2015). IR - infrared.

Figure 6. Methane Infrared Spectrum



Source: Modified from Coblenz Society (2018) NIST Chemistry WebBook.

3.5 LASER SPECTROSCOPY

Often referred to as active IR, Tunable Diode Laser Absorption Spectroscopy (TDLAS) uses wavelengths generated by a diode laser tuned to a single absorption line. Intensity of transmitted radiation over the absorption line is then measured and converted to a concentration (Figure 7) using the Beer-Lambert Law (Figure 8; Wang *et al.*, 2018). TDLAS devices come in portable and fixed variants, such as the MSA Senscient ELDS, Heath RMLD-CS, and SEMTECH HI-FLOW 2 (not yet certified). Accuracy ranges from 5 parts per million per meter (ppm-m) to < +/- 5% of SV with an upper limit range of 10,000 ppm to 50,000 ppm-m depending on the specific model.

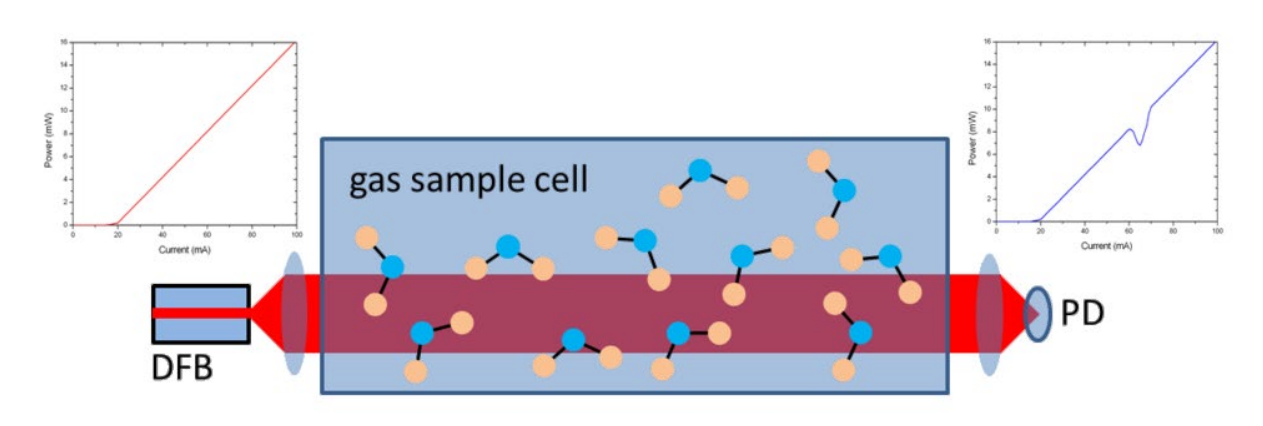


Figure 7. Simplified TDLAS Diagram

Source: Nanoplus (2023). DFB – distributed feedback laser; PD – photodetector.

Figure 8. Beer-Lambert Law

$$I(\tilde{\nu}) = I_0(\tilde{\nu}) \exp(-\alpha(\tilde{\nu})L) = I_0(\tilde{\nu}) \exp(-\sigma(\tilde{\nu})NL)$$

where,

 $I(ilde{
u})$ is the transmitted intensity of the radiation after it has traversed a distance L through the medium,

 $I_0(\tilde{\nu})$ is the initial intensity of the radiation,

 $\alpha(\tilde{\nu}) = \sigma(\tilde{\nu})N = S(T)\phi(\tilde{\nu} - \tilde{\nu}_0)$ is the absorbance of the medium,

 $\sigma(\tilde{\nu})$ is the absorption cross-section of the absorbing species,

N is the number density of the absorbing species,

S(T) is the line strength (i.e. the total absorption per molecule) of the absorbing species at temperature T.

 $\phi(\tilde{\nu}-\tilde{\nu}_0)$ is the lineshape function for the particular absorption line. Sometimes also represented by $g(\tilde{\nu}-\tilde{\nu}_0)$,

 $\tilde{\nu}_0$ is the center frequency of the spectrum.

Source: Wikipedia (2023).

Advances in fixed laser technology that utilize dual frequency comb laser spectrometry (emits and detects light in the near-infrared) in an open-path array such as the LongPath from LongPath Technologies Inc., considers meteorological data in an inversion model to quantify mass emission leak rates as shown in Figure 9 (Alden et al., 2019). Single-blind testing completed at the Methane

Emissions Technology Evaluation Center (METEC) at Colorado State University in Fort Collins, Colorado, at an operating distance of 1 km demonstrated the device quantified leaks ranging from 0-10.7 g/min (0.642 kg/hr) with a mean absolute deviation from true emissions rates of 27% (Alden et al., 2019).

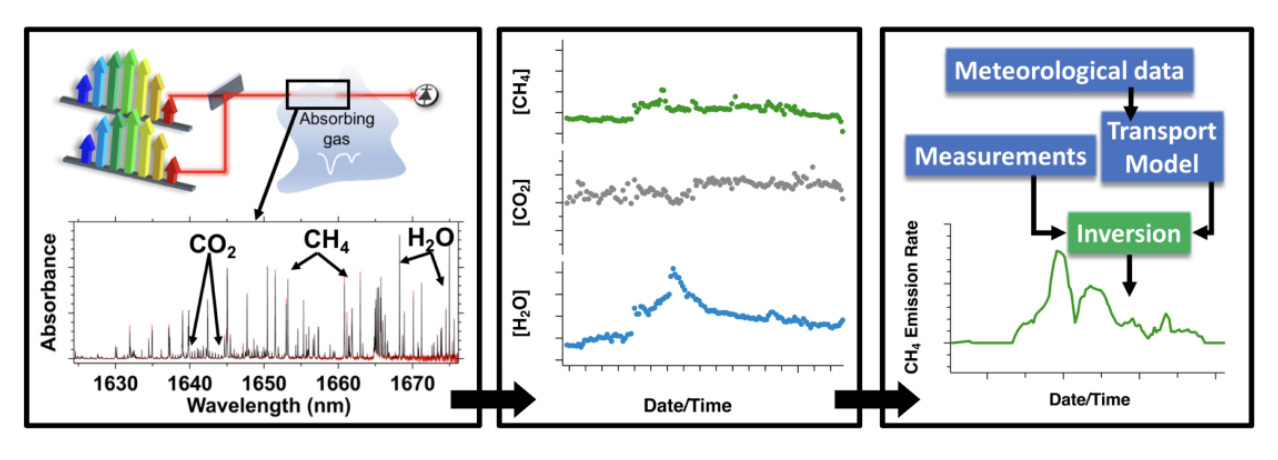


Figure 9. Inversion Processing of LongPath

Source: LongPath (2023).

Laser dispersion spectroscopy involving near- and mid-IR wavelengths, combined with high-resolution differential dispersion spectra, with an open-path gas sensor, processed via Markov-chain Monte Carlo analysis, was able to correctly identify CH₄ sources within 9 m of their actual location in more than 75% of cases (Wiedmann *et al.*, 2022). Accuracy of mass emission rates was strongly correlated to localized accuracy and gave more than a 30% improvement on results in 70% of cases.

3.6 HIGH FLOW SAMPLER (HFS) DETECTION

HFSs are able to capture and measure fugitive CH_4 air streams by using a variety of hose attachments and blankets to enclose the leak source (Figure 10). The devices can determine the concentration of the leak and calculate a volumetric leak rate. The original HFS was introduced to the market in 2001 by Bacharach under the model name HI FLOW Sampler, but after third-party testing had concentration inconsistencies between the switch point of the catalytic to thermal oxidation sensors (Connolly *et al.* 2019). The model has since been discontinued and reengineered by Hetek Solutions Inc. under the model name Hetek Flow Sampler. Flow rate is determined by passing the sample across an orifice plate and concentration is measured using a combination of catalytic- (0-5%) and thermal-oxidation (5-100%) sensors (see Section 3.1 for further discussion). The HFS captures measurements in two stages that are each one minute long. During each stage, a volumetric flow rate (Q_{leak}) is calculated using equation 1. The final output is displayed in actual cubic feet per minute (ACFM) derived from field conditions.



Figure 10. Bacharach HI FLOW Sampler

Source: Intero (2023). The technician is using a blanket and clips to encapsulate the leak before taking measurements with a HFS.

Quantified Leak = Flow Rate
$$\times$$
 (Gas_{sample} - Gas_{Background}) \times 10⁻² (Eq. 1)

where:

Quantified Leak = rate of gas leak from source (cfm or lpm)

Flow Rate = blower flow rate (cfm or lpm)

Gas_{sample} = concentration of gas from leak source (%)

Gas_{background} = background gas concentration (%)

Source: Hetek (2023).

Detectable leak flow rate measurements range from 0.052 to 5.0 cubit feet per minute (CFM) with an accuracy of \pm -5% for both concentration and flow rate. The HFS output value (Q_{leak} or actual

cubic feet per minute) can be used to derive mass emission flow rate (*i.e.*, kg/hr) using equations 3 through 5:

$$SCFM = ACFM * \left(\frac{P_{ACTUAL}}{14.7psi}\right) * \left(\frac{528^{\circ}R}{T_{ACTUAL}}\right)$$
 (Eq. 3)

where:

SCFM = standard cubic feet per minute ACFM = actual cubic feet per minute $-Q_{LEAK}$ P_{ACTUAL} = barometric pressure (psi) T_{ACTUAL} = temperature in Rankine (°R)

Source: Hetek (2023).

 $SCMM = SCFM \times (0.028317 \ scm/scf) \tag{Eq.4}$

Where:

SCM = standard cubic metre SCMM = standard cubic metre per minute

Source: Modified from Hetek (2023).

(Eq. 5)

$$Mass\ Emission\ Rate\ \left(\frac{kg}{hr}\right) = standard\ \left(\frac{m^3}{min}\right)*\ 0.657\ \left(\frac{kg}{m^3}\right)*\ 60\ \left(\frac{min}{hr}\right)$$

Where:

Density of methane = 0.657 kg/m³ at 25°C and 1 atmosphere

At the time of writing, no other known HFS certified devices were currently on the market. SEMTECH is in the final product engineering and certification stage of their HI FLOW 2 sampler which uses TDLAS for concentration measurements and suggests the device can measure a flow rate range between 0.001 – 25 CFM; the methods used to derive flow measurements using this particular device are unpublished.

3.7 OPTICAL GAS IMAGING (OGI)

Currently, an accepted detection tool for CH₄ gas plumes (EPA, 2008; Zeng et al., 2017) often referred to as an Alternative Work Practice (AWP), is an OGI camera use both IR and thermal imaging technology to visualize CH₄ gas plumes in real time on a viewfinder or screen. The quantum detectors and filters in OGIs require internal cryogenic cooling (no higher than -100°C, typically operating at approximately -200°C). Specific to CH₄ gas, OGIs are tuned to operate between 3 to 5 µm and use an indium antimonide (InSb) quantum detector. A spectral filter that

restricts the camera to operate within the spectral band is cooled and placed directly in front of the detector.

The spectral band is unique to each gas as the gas must absorb IR radiation in order for the camera to detect it (FLIR, 2023; Figure 11). To visualize methane on an OGI, three parameters are required: gas has an IR absorption peak (λ) that overlaps with spectral filter of OGI camera, Δ Temperature (T) differential between gas and background, and sufficient concentration-pathlength (CL) (Providence, 2018). To calculate thermal radiance (equation 6), there must be a radiant contrast, and temperature contrast (> 1%), between the methane plume and background (Figure 12).

OGI cameras can come in portable variants such as the FLIR GF77, GF620, GFx320, Opgal EyeCGas 2.0, Opgal EyeCGas Mini, or fixed variants such as the FLIR GF77a, FLIR G300a, and Opgal EyeCGas 24/7 (Pro). Accuracy ranges from +/- 1°C (in 0-100°C ambient temperatures), to +/- 5°C in 15-35°C depending on the specific model. Factors affecting OGI measurements include distance, Δ (T) (gas T – background T), gas composition, strong reflections (glint), and wind (also called dispersion condition).

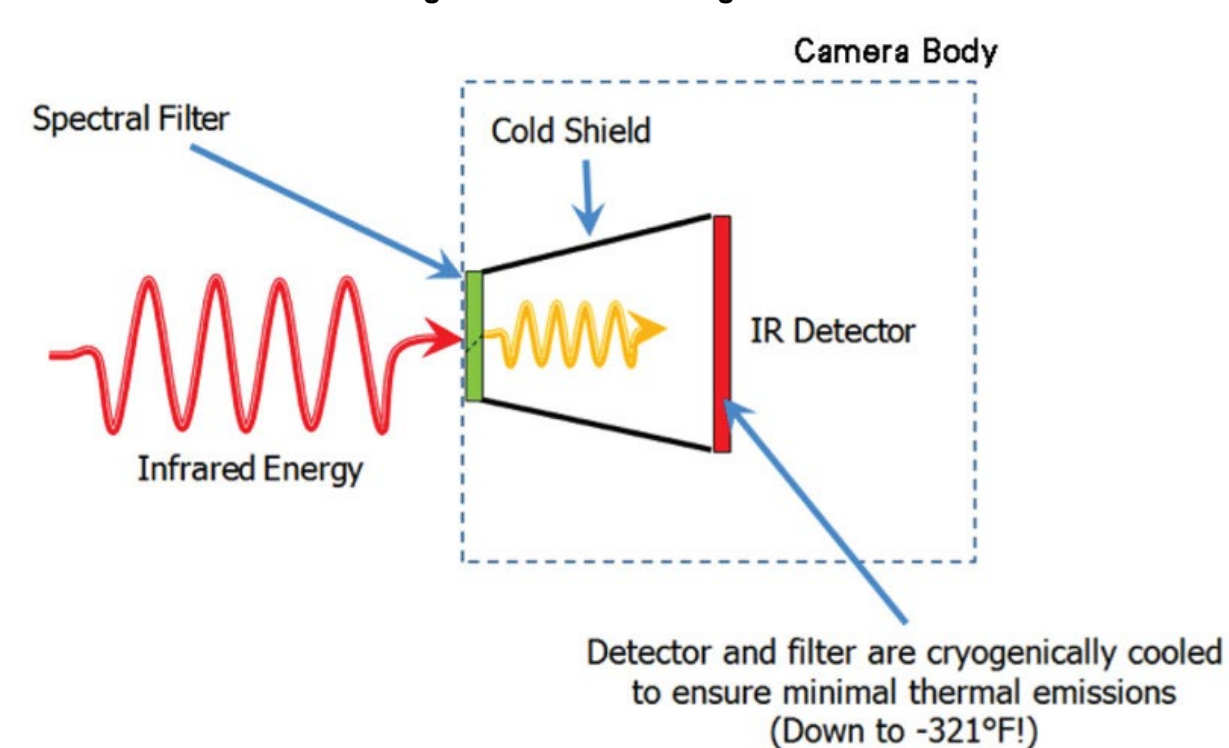
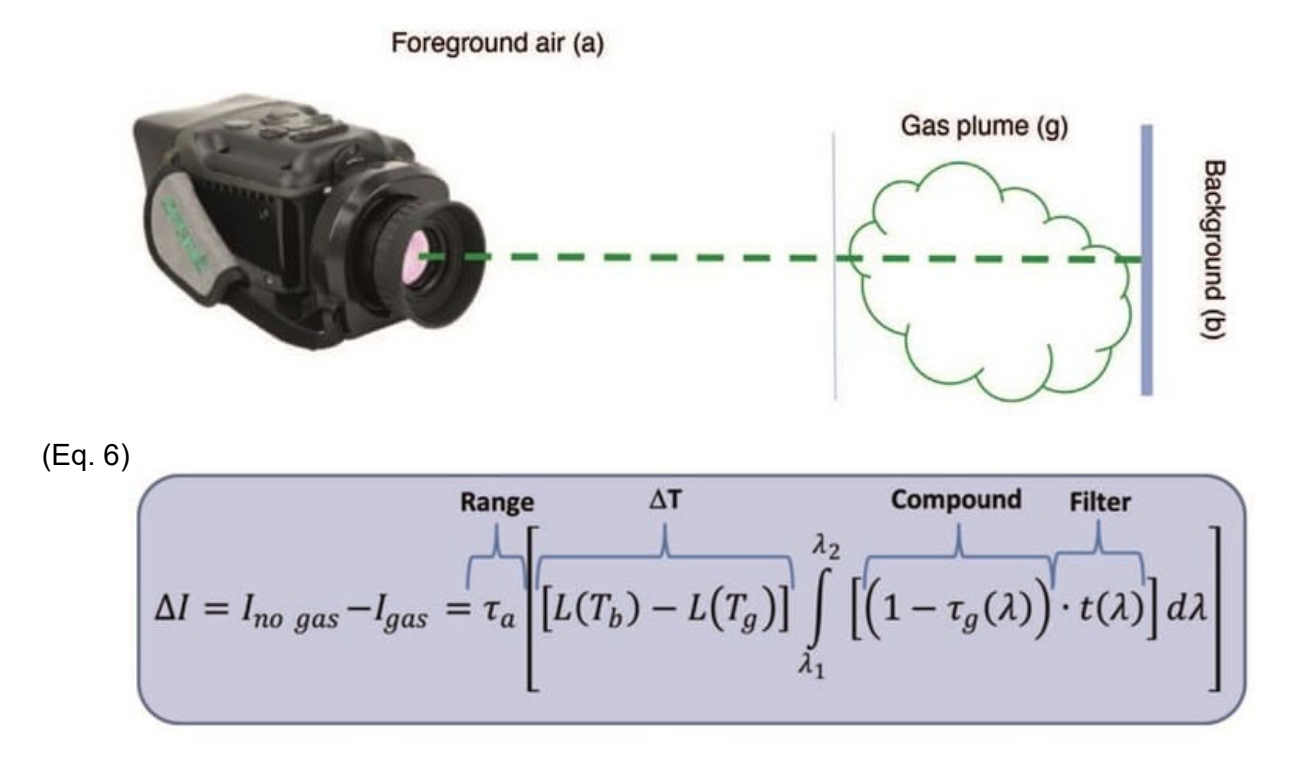


Figure 11. Internal design of an OGI

Source: FLIR (2023).

Figure 12. Calculating Thermal Radiance Contrast for Imaging



 $I_{\text{no gas}}$ – integrated thermal radiance over the bandpass filter spectral range, on pixels with no gas.

Igas - integrated thermal radiance over the bandpass filter spectral range, on pixels with gas.

 $t(\lambda)$ – bandpass filter transmission as a function of wavelength.

I(T) – integrated Planck's function over the bandpass filter spectral range.

Ta - integrated foreground air transmission over the bandpass filter spectral range.

Source: Modified from Opgal (2022).

OGI detection limits are affected by distance and a temperature differential between ambient air and the temperature of a background object, for example a pipe or concrete wall, which can be different depending on the local solar radiation on the day of OGI inspection. Optimal distances to leak source from camera are: 23 mm (6'), 38 mm (10') and 92 mm (20') (Providence Photonics LLC, 2018). Zeng and Morris (2019) determined that a ΔT greater than +/- of 5°C can have profound impacts on detection limits (Figure 13). Absorptive plumes occur when the background T is higher than the gas T, while emissive plumes are the opposite. Maximum allowance distances for methane detection limits of 30 g/hr are summarized in Figure 14 (Zeng and Morris, 2019). OGI cameras can be used on a qualitative basis, detecting leaks/no leaks, size of plumes, *etc.* but require additional software to quantify gas plumes (discussed in Section 3.8).

35,000 30,000 Detection Limit (ppm-m) DL-Propane 25,000 DL-Methane 20,000 15,000 10,000 5,000 0 -20 -15 -10 -5 -25 5 0 10 15 20 25 ΔT (=Background - Ambient, in C or K)

Figure 13. OGI Detection Limits as a Function of Temperature Differential

Source: Zeng and Morris (2019). T – temperature; DL – detection limit; C – degrees Celsius; K – Kelvin.

Figure 14. Distance as a Function of Temperature Differential and Plume Type for a Maximum 30 g/hr Detection Limit

	Absorptiv	ve plume	Emissive	plume
Δ <i>T</i> (°C)	d (m)	d (ft)	d (m)	d (ft)
1	1.28	4.2	1.08	3.5
2	1.87	6.1	1.83	6.0
4	2.73	8.9	3.12	10.2
6	3.40	11.2	4.25	13.9
8	3.98	13.1	5.30	17.4
10	4.50	14.8	6.28	20.6
15	5.62	18.4	8.57	28.1
20	6.57	21.6	10.67	35.0
25	7.43	24.4	12.66	41.5
30	8.20	26.9	14.56	47.8

Source: Zeng and Morris (2019). T – temperature; C – degrees Celsius d – distance; m – meters; ft – feet. Emissive plumes are more sensitive and therefore can accommodate a longer viewing distance.

3.8 QUANTITATIVE OPTICAL GAS IMAGING (QOGI)

QOGI is a developing technology deployed by FLIR and Opgal that uses current OGI devices and adds proprietary software algorithms that evaluate IR contrast intensity (Δ I) on a pixel-by-pixel basis to quantify gas plumes, such as the FLIR QL320 and Opgal EyeCSite 2.0/Pro. A benefit of QOGI is its ability to directly quantify mass emission leak rates in units such as grams per hour (g/h), pounds per hour (lb/h) or megatonnes per hour (MT/h), or volumetric leak rates such as liters per minute (L/min) or standard cubic feet per hour (SCFM) depending on the company used. Concentrations can also be measured in ppm or ppm-m. FLIR (2020) states their device can quantify leaks as low as 11.8 g/hr for methane with a 30% accuracy and is approved to meet regulatory requirements.

Leak rate is determined by taking the inverse of both the pixel contrast intensity of a gas plume vs. background (ΔI), which is a function of ΔT , and the number of pixels that have a higher ΔI -value above a determined threshold. Specific to FLIR, quantification is relative to propane (the refence compound with a response factor of 1.000) and uses a response factor of 0.297 to calculate values for CH₄. While the exact algorithms and RF derivation is proprietary with respect to Opgal and FLIR, Zeng et al. (2017) independently evaluated three methods for deriving RF values and found that RF was not a static value when taking into account CL (Figure 15), and confirmed that RF is not affected by ΔT between gas and background temperatures.

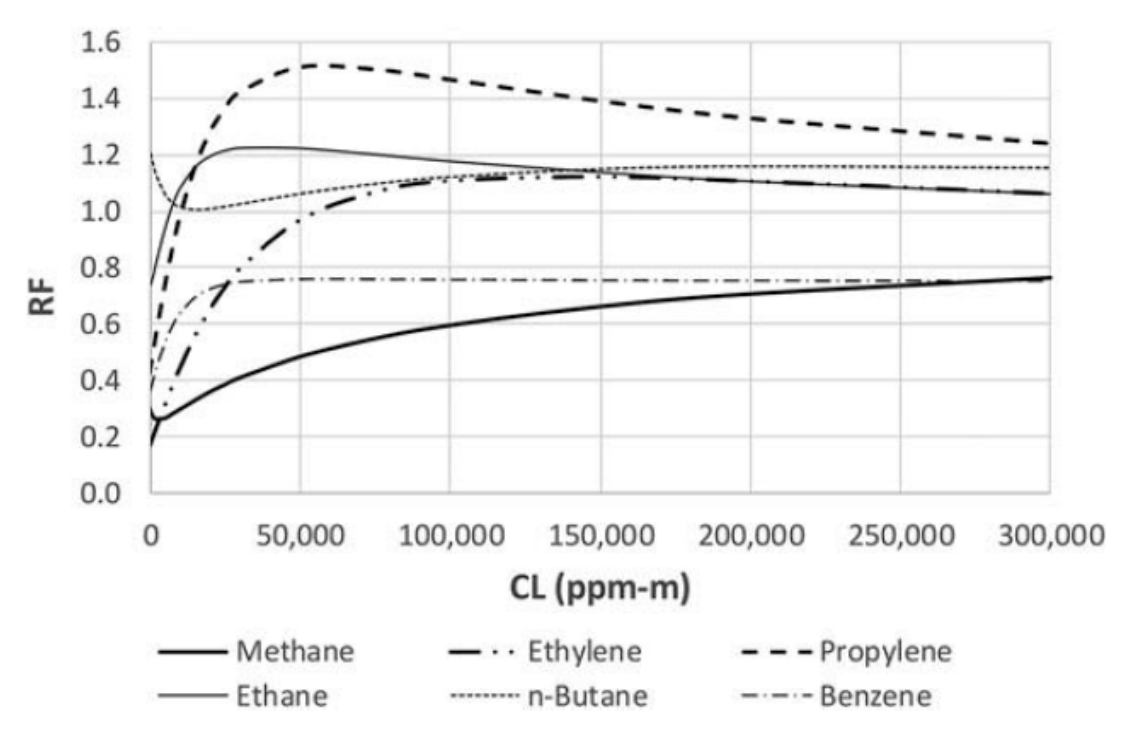


Figure 15. Response Factors as a Function of Concentration Path-Length

Source: Zeng et al. (2019). RF – response factor; CL – concentration path-length.

As QOGI relies on data collected by the OGI camera, the same constraints and considerations apply to most accurately interpret the data, which includes selecting an appropriate background, ΔT between gas and background temperatures and being cognizant of distance to object. Ambient temperature and distance to leak from camera (via laser range finder or measuring tape) must be measured before each data capture.

3.9 LIDAR SENSORS

Light Detection and Ranging (LiDAR) sensors can be mounted on small manned aircraft (plane or helicopter) or unmanned aircraft (drone) to detect methane plumes at sites. Additionally, satellites can aid in aerial surveys, particularly sites which are very remote using resources such as the European Space Agency satellite Sentinel-5P which detects leaks larger than 4,500 kg/hr, or private companies with high resolution satellites such as the SPECTRA GHGSat which detects leaks larger than 100 kg/hr (IEA, 2023). LiDAR is used to detect CH₄ via the differential absorption lidar (DIAL) method which considers two laser lines. One laser is tuned to the absorption wavelength of methane referred to as the 'on' wavelength (λ_{on}), while another is tuned to the wing of the absorption line generally referred to as the 'off' wavelength (λ_{off}). The concentration is then derived from a ratio of the backscattered LiDAR signals as shown in equation 7 and Figure 16 (Yakovley, et al., 2022). Methane with detection limits of 50 parts per billion (ppb) was measured in the 3.3–3.4 µm range at distances of 1 km from a mobile DIAL platform (Innocenti, et. al, 2017). LiDAR is particularly useful in remote locations and extremely accurate, however results can be skewed from changes in wind and wind direction (Figure 17), surface terrain reflectance, and can affected by overhead commercial aircraft (EPA, 2011). Detection of methane is characterized as statistical events and therefore a critical aspect of quantifying mass emission rates is tied to the probability of detection (PoD), or confidence level of detecting a leak. Caution should be applied to the minimum detection limit as smaller leaks tend to have lower PoDs, which could introduce false positives if the PoD is not sufficiently confident (Bridger Photonics, 2023).

$$\frac{I(\lambda_{on},R)}{I(\lambda_{off},R)} = \exp\left\{-2\int_{0}^{R} N(r) \left[\sigma(\lambda_{on}) - \sigma(\lambda_{off})\right] dr\right\}$$
 (eq. 7)

Where:

 $I(\lambda_{on},R)$ – backscattering intensity for on-wavelength

I(λoff,R) – backscattering intensity for off-wavelength

R – detection distance

 $\sigma(\lambda_{on})$ – absorption cross-section for on-wavelength

 $\sigma(\lambda_{\text{off}})$ – absorption cross-section for off-wavelength

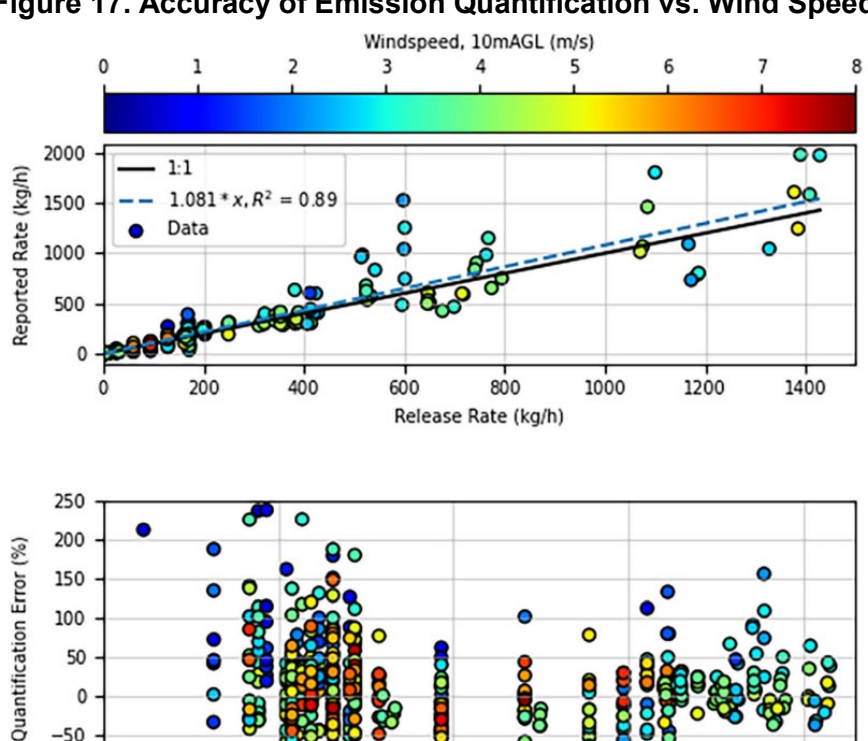
N(r) – gas concentration at distance (r) and

Source: Modified from Zhao et al. 2013.

Free Troposphere λ_{on} λ_{off} λ_{hsrl} λ_{hsrl} Boundary Boundary Layer Layer Scatter Surface Scatter >90% Pulse Overlap

Figure 16. Overview of DIAL Methodology on Aircraft

Source: Barton-Grimley et al. 2022.



Release Rate (kg/h)

100

1000

Figure 17. Accuracy of Emission Quantification vs. Wind Speed

Source: Modified from Bell et al. 2022. Coloured dots correspond to measured windspeed (m/s).

50 0 -50 -100 0.1

4 PPMV AND CFM REGRESSION ANALYSIS

4.1 Mass Emission Correlation Equations

Various groups have completed linear regression analyses between ppmv concentrations and volumetric flow rates for VOCs, CH₄, or CH₄-emitted from various types of industrial infrastructure. Typical leaking sources or components consist of valves, connectors, flanges, regulators, meters, open-ended lines, and actuators (US EPA, 1995; Sage, 2019; Ke *et al.*, 2020; Equilibrium, 2022).

Currently, Canadian regulatory law cited in SOR_2018-66 § 3.4 mirrors the petroleum industry specific concentration to mass emission rate (kg/hr) equivalency formulae derived by the EPA (1995), as summarized in Table 1. Screening values are to be used in the correlation equations as default emission rates can be based on pegged values (concentrations above the upper limit of measurement for a device).

Emission equivalency linear regression analysis was completed by Sage ATC Environmental Consulting LLC (Sage, 2019) for the California Air Resource Board (CARB) as a means to refine EPA (1995) and California Air Pollution Control Officers Association (CAPCOA) (1999) emissions estimates for natural gas facilities. CAPCOA (1999) advises an average emissions factor to screening value concentrations below 10,000 ppmv. A second emissions factor for concentrations above 10,000 ppmv was derived. The EPA (1995) equivalency formulae could be used for SVs between 1 – 10,000 ppmv or at 100,000 ppmv, depending on the local district regulations.

Sage (2019) used a combination of Method 21 approved devices, the Thermo Scientific TVA-1000B and Bacharach Hi-Flower Sampler, to measure 160 components at 39 sites in 2015. The Hi-Flow Sampler was calibrated to CH₄ for reporting CH₄ concentrations. Using a log-log regression model for each component type, emission equivalency formulae were derived (Table 1) for natural gas production and processing facilities, which were at least an order of magnitude different than the EPA's. Figure 18 shows the confidence of the derived equations for each component. A summary of the EPA and CARB equivalency equations are found in Table 1.

Table 1. Summary of Equivalency Formulae to Calculate Mass Leak Rate from Concentration and Relative Percent Difference

Component Type	Mass Lea	Relative Percent		
Component Type	EPA, 1995	Sage, 2019	Difference (%)	
Valve	2.29E-06 x SV ^{0.746}	1.3236E-05 x SV ^{0.8118}	165.5	
Connector	1.53E-06 x SV ^{0.735}	1.5523E-05 x SV ^{0.6848}	145.9	
Flange	4.61E-06 x SV ^{0.703}	3.6815E-03 x SV ^{0.3369}	185.9	
Flanges and Connectors	-	4.1772E-04 x SV ^{0.4666}	-	
Open-ended Lines	2.20E-06 x SV ^{0.704}	8.1490E-05 x SV ^{0.7157}	190.5	
Other	1.36 E-05 x SV ^{0.610}	2.2542E-05 x SV ^{0.7902}	158.8	

Notes: Sourced from EPA, 1995 and Sage, 2019. SV – screen value in ppmv. Correlations predict methane-equivalent Total Organic Compound (TOC) emission rates at standard conditions of 25°C and 1 atmosphere. Generic screen value of 10,000 ppmv was used for all calculations to determine relative percentage difference.

Figure 18. Gas Correlation Model Parameters

	2015 CARB Study						
Component Type	Gas Service Natural Gas Production Sites						
	N	SBCF	β_0	β_1	\mathbf{r}^2		
Valves	33	8.6458	-5.8151	0.8118	0.609		
Connectors	37	3.6238	-5.3682	0.6848	0.635		
Flanges	22	17.9752	-3.6886	0.3369	0.185		
Connectors & Flanges	59	10.1848	-4.3871	0.4666	0.352		
OELs	34	4.4355	-4.7358	0.7157	0.753		
Other	34	4.2958	-5.2801	0.7902	0.645		

N = Number of Samples

SBCF = Scale Bias Correction Factor, for log10 values

 β_0 = Intercept of regression line

 β_1 = Slope of regression line

 r^2 = Coefficient of determination

Source: Sage (2019).

Cheadle et al. (2022) published a large-scale data analysis compromised of nearly two million components measured at over 300 facilities as part of an LDAR program in California from 2018 to 2019 using approved Method 21 devices. Components reported to CARB were likely handling gas and therefore using the EPA (1995) emission equivalency equations, which use the screen value concentration data where available, would have resulted in an under-estimation of mass emission leak rates, as EPA correlation equations were developed based on measurements of components handling gas, light oil, and heavy oil. Therefore, the most appropriate correlation equations for primarily gas-handling facilities were the correlation equations derived in Sage (2019) as they were more conservative in comparison to EPA (1995).

4.2 DATASET ANALYSIS

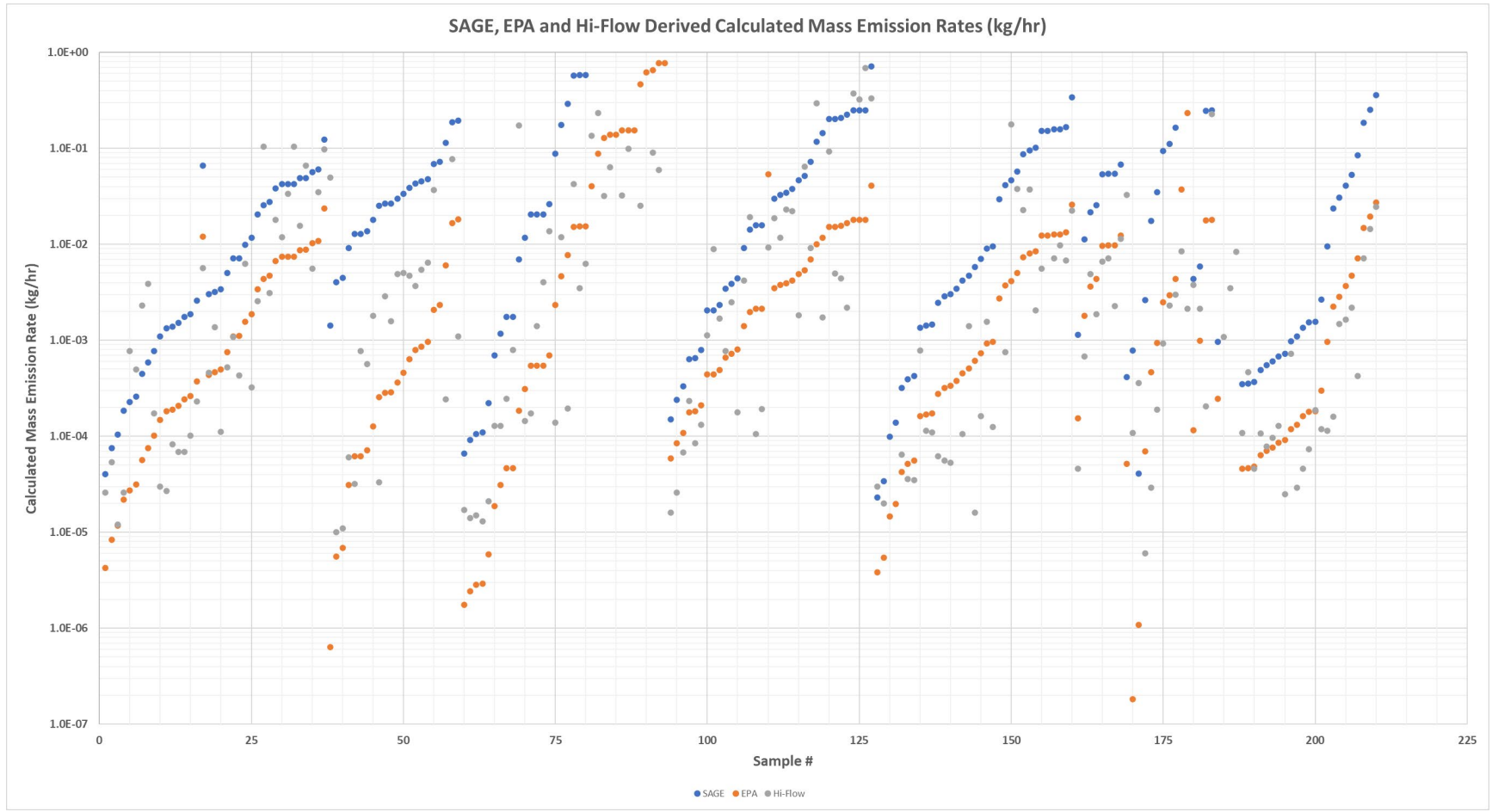
4.2.1 SAGE DATASET

The Sage (2019) database captured Method 21 (EPA, 2017) concentration measurements via a Thermo Scientific TVA 1000B device displayed in ppm using a FID sensor. Simultaneous measurements were also collected using the now discontinued Bacharach HI FLOW sampler, which displayed concentrations as a percentage using a combination of catalytic- (0-5%) and thermal-oxidation (5-100%) sensors. Time and date stamps were provided and the tests were generally completed near simultaneously between the two devices. As discussed above, the dataset was compromised of 160 components taken at 39 sites measured in 2015 at natural gas processing facilities.

Figure 19 shows results for the dataset. Results are shown from the Sage (2019) dataset measured via Method 21, converted to kg/hr mass emission rate using the equations provided by Sage (2019) that are more specific to natural gas. Values in kg/hr calculated from the less specific US EPA (1995) equations (equivalency formulas) applied to the Sage (2019) dataset are also shown. Finally, results from the Bacharach HI FLOW sampler in units of kg/hr are shown.

Calculated mass emission rates based on the Method 21 measurements processed via the Sage (2019) algorithms had greater alignment with the Bacharach measurements in comparison to the US EPA (1995) derived values, a result that was not unexpected. Although a rough correlation was observed between the Sage (2019) calculated mass emission rates and Bacharach measured rates, the variance was relatively large and spanned more than an order of magnitude.

Figure 19. Comparison of Calculated Mass Emission Rates Using Concentration Data on a Logarithmic Scale



Notes: Sourced from EPA, 1995 and Sage, 2019. The Y-axis is on a logarithmic scale. Blue – SAGE, EPA – Orange, Grey – Hi-Flow.

MIDSTREAM NATURAL GAS TRANSMISSION DATASET

Equilibrium (2022) completed a linear regression analysis between concentration (ppmv) and flow rate (cfm) data from a private database comprised of 134 unique entries. The data were sourced from a midstream company. Sources/components consisted of predominantly valves (54%), connectors (30%), actuators (2%) and regulators (2%); the remaining 12% was part of an ambiguous 'other' category and omitted from analysis. Concentration data was collected using an RKI Eagle 2 and flow rate data was collected using a Bacharach Hi Flow sampler. Values were converted to a log-log scale to reduce the magnitude of variation within the dataset. The results for valves are presented in Figure 20.

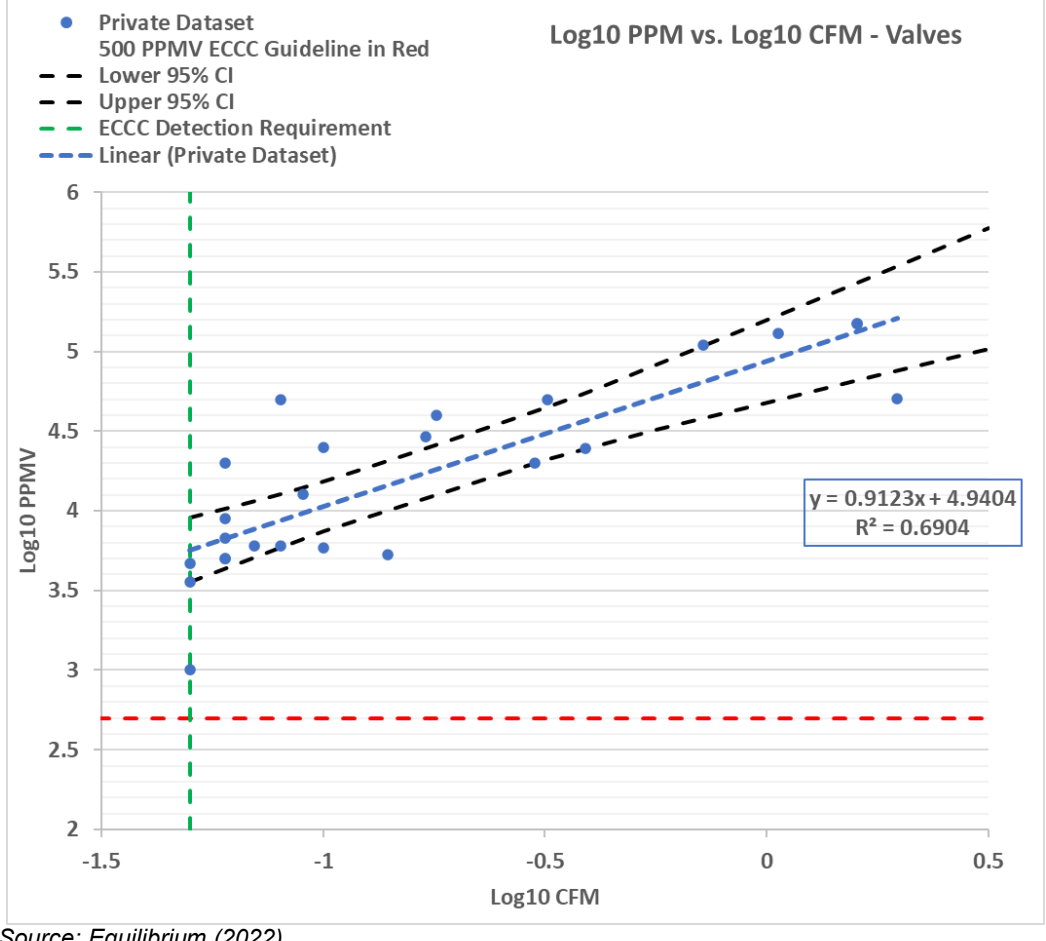


Figure 20. Linear regression of Log10 CFM Versus Log10 PPMV Values for Valves

Source: Equilibrium (2022).

A comprehensive goodness-of-fit evaluation was completed on flow rate data to determine if different component and sub-component types could be attributed to statistically significant data distribution curves. The Kolmogorov-Smirnov (K-S) statistical test can be used to evaluate empirical cumulative distribution functions (or probability density function) and is described by the following equation:

$$F_n(x) = \frac{1}{n} \cdot \left[\text{Number of observations} \le x \right]$$
 (Eq. 8)

Source: EasyFit™ Manual

The test involves the generation of a Kolmogorov-Smirnov statistic (D in equation 9 below), which is based on the largest vertical difference between the theoretical and the empirical cumulative distribution function and describes essentially the goodness of fit:

(eq. 9)

$$D = \max_{1 \le i \le n} \left(F(x_i) - \frac{i-1}{n}, \frac{i}{n} - F(x_i) \right)$$

Source: EasyFit™ Manual

Other statistical tests were evaluated such as the Anderson-Darling Test (A-D) and Chi-Squared Test (Chi2). The A-D test has an 'emphasis' on the 'tails' of the distribution, which has a lesser relevance for flow rate analysis that is examining central tendencies – as a result, the K-S test received a greater focus for assessing significance. The Chi2 test is more sensitive to sample size.

K-S testing was completed using the software program EasyFit™ to determine if the null hypothesis would be rejected (Yes or No) at alpha (α) values of: 0.2, 0.1, 0.05, 0.02, and 0.01. A statistical value was then calculated for each of the probability distribution type and ranked, with the lowest statistical K-S value as rank #1. This process allowed for the identification of distribution types that may describe the dataset with statistical significance and can be used to predict likely ranges in potential leak rates for different Component/Source and Sub-source types. The EasyFit™ analysis covered a relatively large number of different distribution types (e.g., General Logistic, Wakeby, Gamma, Weibull, Lognormal, Normal, General Extreme Value, etc.). Table 2 summarizes the top-ranking distribution, K-S statistic and P-value for each source/component and sub-source.

Table 2. CFM Dataset Summarized Results from EasyFit™ Goodness of Fit Modelling

Source/ Component	Sub source	Sample Size	Data Type	K-S Statistic	K-S P-Value	No -Rejection K-S Test?	Sub-Source Rank #1 Distribution	No- Rejection ALL Tests?	Source / Component Best- Fit Distribution	Comments
Actuator	ALL	14	Leak Rate (CFM)	0.12798	0.95354	✓	Gen. Logistic	✓	Gen. Logistic	
Actuator	ALL	14	Log10 CFM	0.11628	0.98001	✓	Wakeby	✓	Gen. Logistic	
Connector	Valve Body	14	Leak Rate (CFM)	0.20781	0.51515	✓	Pearson 5 (3P)	✓	Burr	
Connector	Valve Body	14	Log10 CFM	0.19031	0.62438	✓	Gen. Logistic	✓	Log-Logistic (3P) and Gen. Logistic	
Connector	Threaded Connection	50	Leak Rate (CFM)	0.12266	0.40661	✓	Burr	✓	Burr	
Connector	Threaded Connection	50	Log10 CFM	0.12517	0.38192	✓	Wakeby	✓	Log-Logistic (3P) and Gen. Logistic	
Regulator	ALL	8	Leak Rate (CFM)	0.15233	0.98757	× (K-S & A-D)	Gen. Logistic	× (K-S & A-D)	Johnson and Gen. Extreme Value	Small sample size resulted in no Chi-
Regulator	ALL	8	Log10 CFM	0.15394	0.98618	× (K-S & A-D)	Uniform	× (K-S & A-D)	Johnson and Gen. Extreme Value	Squared distributions
Valve	Valve Body	27	Leak Rate (CFM)	0.16925	0.37894	✓	Frechet	✓	Wakeby and General Pareto	Fitting an overall
Valve	Valve Body	27	Log10 CFM	0.15762	0.46655	✓	Wakeby	× (K-S)	Wakeby	Source/Comp onent
Valve	Valve Seat	16	Leak Rate (CFM)	0.13073	0.91483	✓	Burr	✓	Wakeby and General Pareto	distribution was selected
Valve	Valve Seat	16	Log10 CFM	0.12744	0.92824	✓	Phased Bi- Weibull	× (K-S & Chi- Squared)	Wakeby	on individual Sub-Source best-fits,
Valve	Valve Stem	56	Leak Rate (CFM)	0.1088	0.48759	√	Gen. Extreme Value	✓	Wakeby and General Pareto	despite the main Source/Comp
Valve	Valve Stem	56	Log10 CFM	0.13445	0.24097	√	Wakeby	× (K-S & Chi- Squared)	Wakeby	onent (Valve) not fitting any distribution due to 'Yes' rejections.

Notes: Green shaded cells indicate an EasyFit™ statistical calculations which resulted in No-Rejections across all testing methods, indicating a very strong result. Yellow shaded cells indicate at minimum the K-S test resulted in No-rejections across all α-values but did receive a Yes-rejection for other testing methods (still strong result, but not as strong relative to green shaded cells). Orange shaded cells identify a smaller sample size, which resulted in no Chi² distributions.

5 TECHNOLOGY DISCUSSION

Advancements in area-wide methane detection technology have expedited detection and repairs rates, such that the EPA (2016) has determined OGI and Method 21 both provide reliable data for emissions reporting. Several factors can affect the concentration obtained using a Method 21 device, such as geometry of the component, pressure inside the apparatus, wind speed and atmospheric turbulence, which can produce leak rate errors ranging from -80% to +300% as errors propagate (Moati-Abdel et al., 2015).

Method 21 used in LDAR inspections have drawbacks, such as monitoring personnel are required to be physically close to components or sources for inspection to collect samples. In contrast, OGI technology does not require close worker exposure to gas leaks and results can be collected at distance. Furthermore, Method 21 data in LDAR programs captures one point in space, at one time and may not be fully representative of the leak and its varying emission contribution. In contrast, OGI results are for a larger area, over time, but require mathematical processing of the data to predict leaking concentrations.

Quantifying leaks on a mass emission rate basis with improved accuracy and detection, is of value to industry. Differences in concentration to flow rate equivalency calculations that vary by specific component type as well as other factors, have introduced potentially order of magnitude more uncertainty when quantifying fugitive mass emissions (Cheadle *et al.*, 2022). Direct mass emission rate measurement equipment can potentially resolve much of this uncertainty. However, these technologies are still under development and there are limitations. For example, the Hi Flow Sampler is successful at quantifying emissions on a mass flow rate basis, however, the equipment has a maximum reliable flow rate reading of 5 CFM Q_{leak}, above which point measurements become questionable.

5.1 THIRD PARTY METHODS EVALUATION

Third-party field testing and single-blind studies help build confidence for manufacturers and regulatory bodies while helping operators fine-tune detection methods that are effective and accurate for site-specific monitoring and compliance. Three examples are discussed in Sections 5.1.1 to 5.1.3.

5.1.1 CONCAWE EUROPEAN FIELD STUDIES

The Concawe Air Quality Management Group's Special Task Force completed two field testing events (Concawe 2015, 2017). Concawe (2015) completed LDAR testing at two large-scale European refineries that handle gas and light hydrocarbons, which determined that both OGI (FLIR GF320) and point-source Method 21 methodologies were largely in agreement when finding the largest portion of accessible total VOC mass emissions; OGI then could be applied as a standalone method. Controlled leak testing demonstrated that OGI cameras in real conditions were able to find the majority of leaks above 0.0015 kg/hr, however this requires the operator to find this leak which on the OGI camera is visually easier for larger leak sizes.

Concawe (2015) heeded caution for using Method 21 emission factors and correlations as the formulae were developed when the occurrence of large-scale leaks was statistically more frequent and have not taken into account technological advancements. Testing at one site was completed on 74 components using devices Hi-Flow Sampler and a TVA-1000B, which determined that total mass emissions using Method 21 correlations were more than 10 times higher for pegged measurements than the emissions measured directly by the Hi-Flow Sampler (Figure 21).

Figure 21. Leak Rate Estimation

		HFS	M21	HFS	M21
	Number of leaks	Total Emi	ssions (kg/h)	Average	Emissions (kg/h)
Pegged	33	0.25	3.59	0.01	0.112
Non- Pegged	41	0.08	0.132	0.002	0.003
Total	74	0.33	3.73	NA	NA

Source: Concawe (2015).

Additional field testing of OGI cameras (FLIR GF300/320) and quantification module (FLIR QL100) was completed by Concawe (2017) at the VITO LDAR training facility in Mol, Belgium. The QOGI system is referred to as the OGI camera in tandem with the quantification module. Results indicated that the OGI camera could detect all 61 releases with temperature variances as low as 1°C between gas and background. However, the quantification module required a temperature variance of >5°C and provided 31 leak rates out of 61 releases with an average leak rate quantification error of 6% of calculated vs. actual.

Concawe (2017) determined that using the EPA (1995) equivalency formulae from screening values with the same magnitude could represent massive emission rates with several orders of magnitude difference and were generally a poor correlation on a point-to-point basis until large site surveys (*i.e.*, refineries) could be completed in order to average the magnitudes of difference among individual concentration readings. Using Method 21 screening values, only 31 of 61 leak releases could be measured due to flame-out (concentration too high to read, even when using a dilution probe); results of using calculated emission rates from Method 21 SVs are shown in Figure 22. Conversely, using the QOGI system yielded significantly better results (Figure 22).

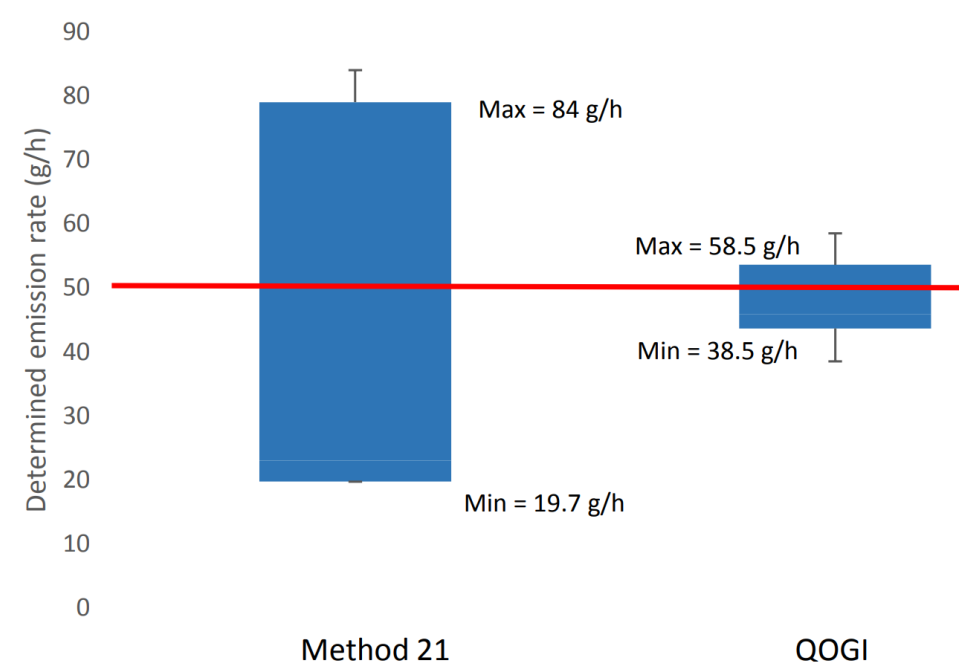
Figure 22. Comparison of Method 21 vs QOGI of Calculated Emissions and Known Release Rates

QOGI vs. Method 21 – Comparison of differences between calculated emissions and known release rates					
Difference ¹ QOGI Method 21					
Minimum	-23%	-92%			
Average	6%	31%			
Standard deviation	22%	155%			
Median	2%	-4%			
Maximum	69%	667%			

Source: Concawe (2017). ¹Difference = (calculated emission rate – release rate) / release rate (%).

To directly compare similar leaks for each method, a common leak rate (0.05 kg/hr) was used. Figure 23 illustrates the statistical range of each method using a box and whiskers plot, while Figure 24 illustrates the calculated mass emission rate using controlled release rates.

Figure 23. Determined Mass Emission Rate (g/h): Method 21 vs. QOGI



Notes: Concawe (2017). g/h – grams per hour. Method 21 (Thermo Scientific TVA 1000B) mass emission rate calculated using EPA (1995) formulae, in contrast to QOGI which used the FLIR Q100 proprietary calculations.

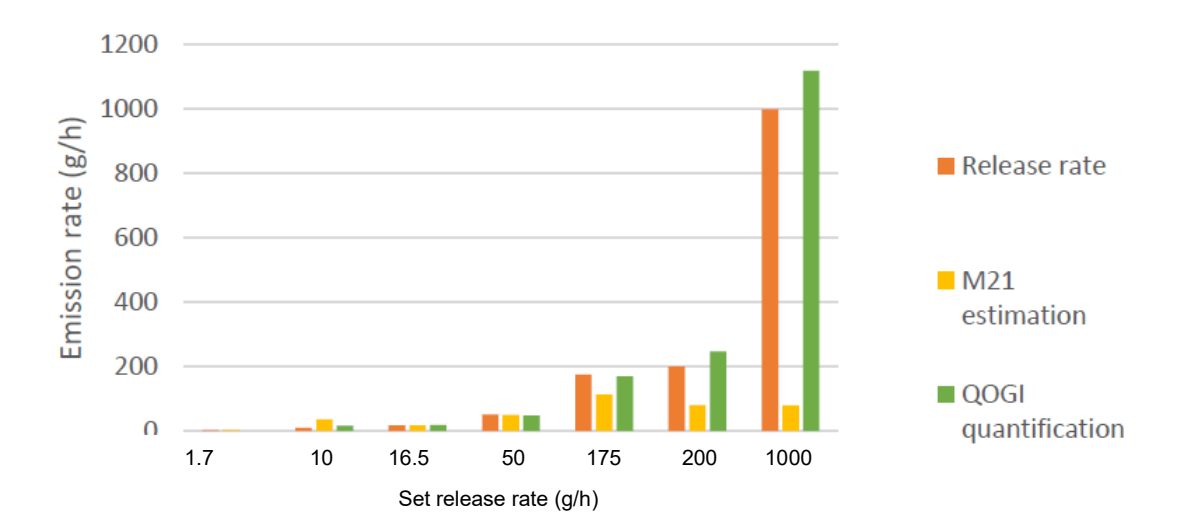


Figure 24. Accuracy of Calculated Mass Emission Rate (g/h): Method 21 vs. QOGI

Notes: Modified from Concawe (2017). g/h – grams per hour. Method 21 (Thermo Scientific TVA 1000B) mass emission rate calculated using EPA (1995) formulae and emission factors compared to the QOGI system which used the FLIR GF320 OGI camera and with quantification module FLIR Q100. Above 175 g/h release rates, Method 21 equivalency estimates showed vastly under-represented calculations while QOGI showed strong agreement across the range.

5.2 ALBERTA METHANE FIELD CHALLENGE

Emerging methane technology (early-stage development) from nine methane detection organizations was independently field tested at 50 facilities near Rocky Mountain House, Alberta, Canada between June 11-21, 2019 and November 14th to 24th, 2019 (Ravikumar *et al.*, 2020). Results indicate that in controlled testing scenarios during phase 2, QOGI had an aggregate error of 18% across a sampling range of 0.198 – 57.6 kg/hr, which in contrast to the Hi Flow sampler, had an approximately 10% aggregate error but an order of magnitude smaller upper sampling range limit (9.21 kg/hr). QOGI demonstrated that the technology is a viable and expedited alternative for quantifying emissions (Figure 25).

Aerial and truck-based systems demonstrated an increased speed over other ground-based technologies at site-wide detection capabilities which would expedite the identification of high-emitting leaks. However, these methods required additional inspection to find the specific leaking component and quantification to determine if a repair was required. Drone and aerial teams were effective at ranking site-wide CH₄ emissions and assessing in inaccessible locations, however their quantification values were different. Overall, quantification amongst the participating teams showed significant variation.

Fixed laser systems generate a large database in short time capturing site-wide data, including methane concentration path-length, wind speed, and direction. Significant efforts are required to process the large amounts of data for actionable information but showed potential for continuous monitoring of localizing leaks. Results from Phase 1 are show in Figure 26.

Figure 25. Parity Chart of Controlled Tests vs. QOGI Readings

Source: Ravikumar et al. (2020).

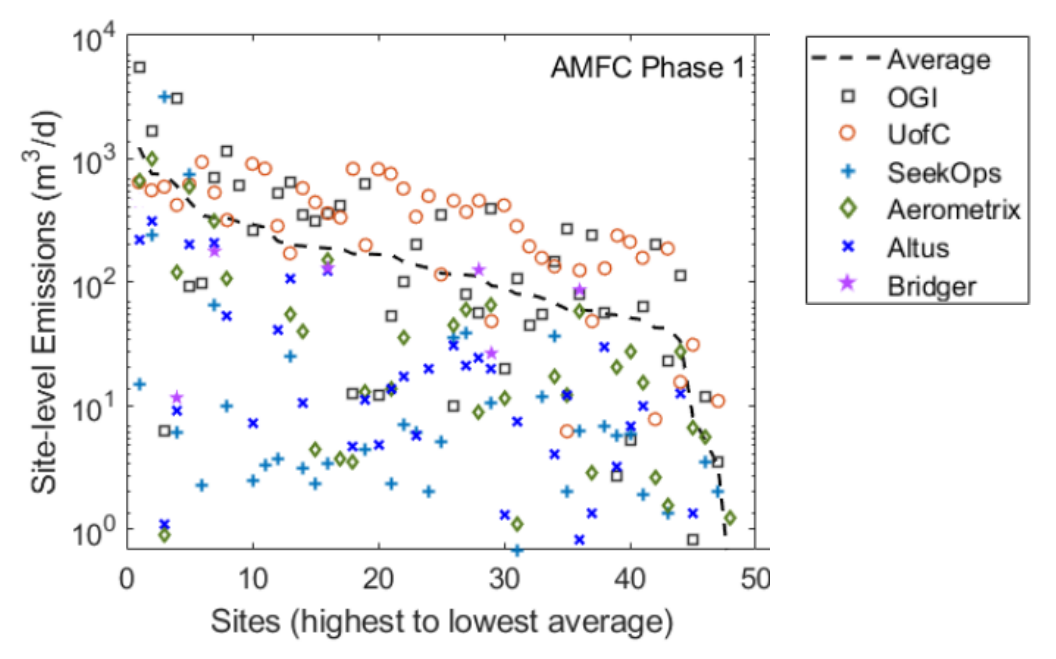


Figure 26. Summary of AMFC Phase 1 Results

Source: Modified from Ravikumar et al. (2020). Sites indicated along x-axis are arranged from highest (left) to lowest (right) with average emissions detected by all teams as the black dashed line.

5.3 METEC EVALUATION OF DUAL FREQUENCY COMB SPECTROSCOPY

Dual frequency comb spectroscopy (DCS) was briefly discussed in Section 3.5 (Laser Spectroscopy). LongPath Technologies completed single-blind testing at the METEC (Methane Emissions Technology Evaluation Center) facility in Fort Collins, Colorado in conjunction with Colorado State University Energy Institute (Alden et al. 2019) of their LongPath DCS device. The testing facility is important because it allows manufacturers to test their equipment with academic experts in real-world scenarios. A single-blind testing protocol is when true emission rates and locations are only known to the testers (University officials) and hidden from the equipment operators. Over a three week period in August and September 2017, a total of three sites compromising of pad- and battery-level were tested. Of 18 tests, the system detection 17 of 17 true leaks and 1 of 1 no-leak scenarios resulting in a 100% success rate, including leaks that were as small as 0.0031 kg/hr. Results of the testing are illustrated in Figure 28 and show promise even for very small emission rates from a distance of >1 km. An operator with numerous small-scale sites in close proximity could allow a 'grid' (Figure 29) of detection devices to be continuously monitoring and flag instances of high-emitting events immediately instead of waiting to be found during regulated inspection intervals.

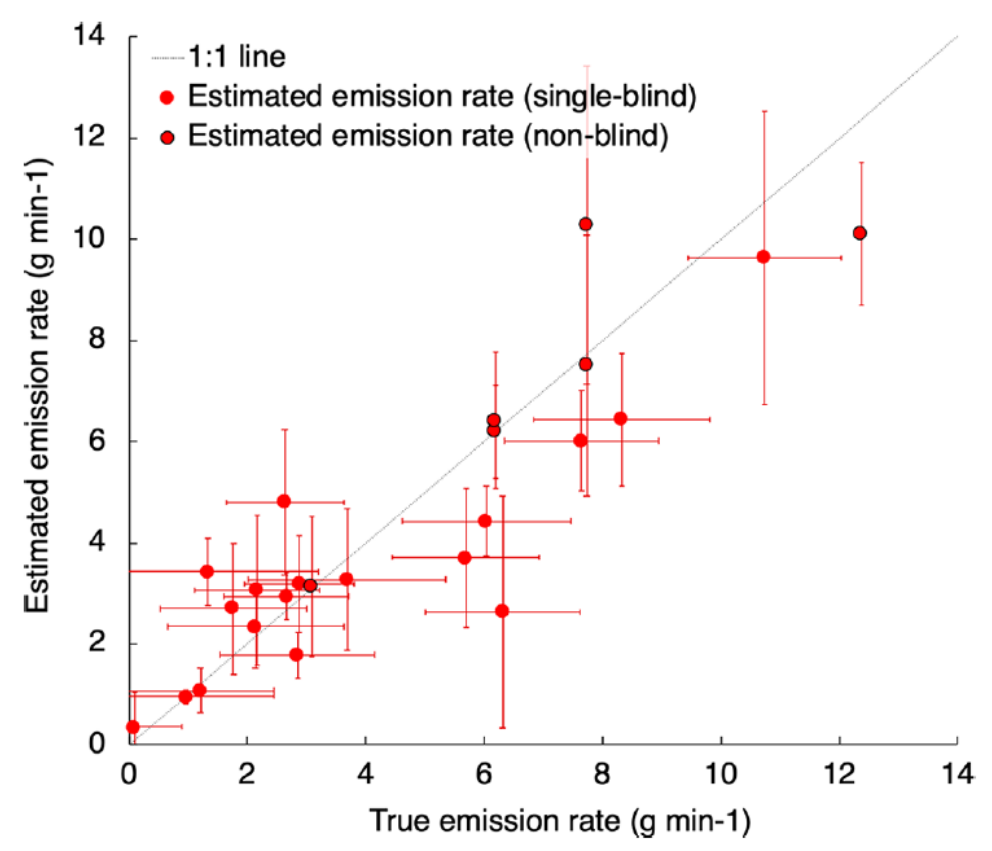


Figure 28. Single-Blind Results from LongPath's Calculated Quantification at METEC

Source: Alden et al. (2019). 2-σ uncertainty on x- and y-axes.

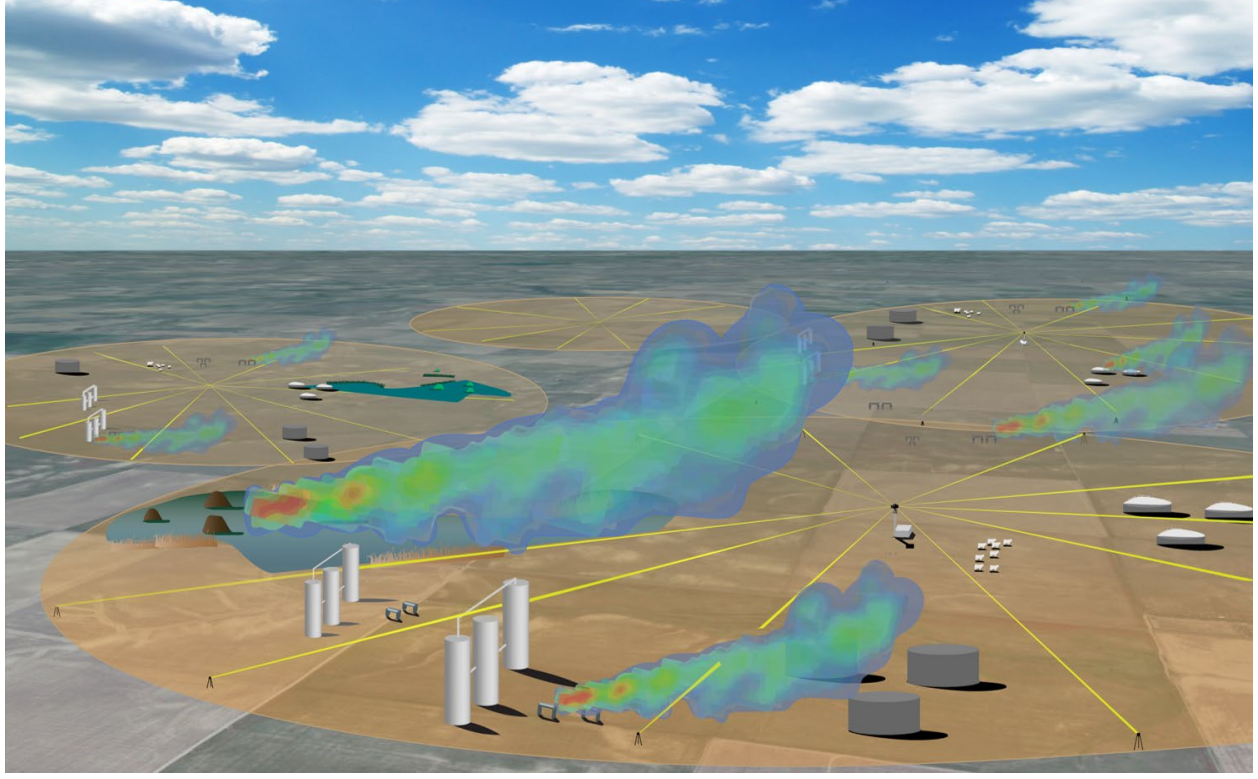


Figure 29. Fixed Dual Frequency Comb Spectroscopy Configuration

Source: Sizemore (2023).

6 RECOMMENDATIONS FOR THE OIL AND GAS SECTOR

6.1 EMISSIONS REPORTING BACKGROUND

As of 2004 under section 46 of the *Canadian Environmental Protection Act* (CEPA) (ECCC, 1999), the Greenhouse Gas Reporting Program (GHGRP) collects information on greenhouse gas (GHG) emissions from facilities across Canada. A facility is defined as "an integrated facility, a pipeline transportation system, or offshore installation." Facilities that emit 10,000 tonnes or more (the "threshold") of total GHGs, in carbon dioxide equivalent units per year, are required to submit a report for each calendar year.

The GHGs included for reporting are carbon dioxide (CO_2), methane (CH_4), nitrous oxide (N_2O), hydrofluorocarbons (HFC), perfluorocarbons (PFC) and sulphur hexafluoride (SF_6). Each GHG must be individually converted to a CO_2 equivalency (CO_2e) via the tonnage of each GHG adjusted by their respective 100-year Global Warming Potential (GWP; ECCC, 2023; IPCC, 2013). This provides the total CO_2e GHG tonnage (Equation 7). If this value is above the threshold, the facility must submit a mass emission report. GWP values for each GHG can be viewed in Table 1 of the *Technical Guidance on Reporting Greenhouse Gas Emissions* (ECCC, 2023). Methane has a GWP of 28. Any facility that falls below the threshold is not required to submit their emissions but encouraged to submit voluntarily.

Equation 7

$$Total\ Emissions\ (in\ CO_{2}\ eq) = \sum_{1}^{l} (E_{CO2} \times GWP_{CO2})_{l} + \sum_{1}^{l} (E_{CH4} \times GWP_{CH4})_{l} + \sum_{1}^{l} (E_{N2O} \times GWP_{N2O})_{l} + \sum_{1}^{l} (E_{HFC} \times GWP_{HFC})_{l} + \sum_{1}^{l} (E_{PFC} \times GWP_{PFC})_{l} + \sum_{1}^{l} (E_{SF6} \times GWP_{SF6})_{l}$$

(ECCC, 2023)

Where:

E = total emissions, from all activities occurring at the facility, of a particular gas from the facility (tonnes)

GWP = global warming potential of the particular gas (Table 1 of Technical Guidance on Reporting Greenhouse Gas Emissions (ECCC, 2023))

i =each emission source

To determine annual tonnage of methane at a facility, five direct or estimation methods may be used which include monitoring or direct measurement, mass balance, emission factors, or engineering estimates.

- 1) Monitoring or Direct Measurement:
 - Monitoring Direct measurements over an extended or uninterrupted period. The
 most accurate method for reporting actual tonnage of methane which can also be
 used later to derive predictive monitoring models that are facility-specific
 - b. Predictive monitoring Correlations developed between measured emission rates and process parameters
 - c. Source testing stack sampling
- 2) Mass Balance: Emissions are determined from the difference in input and output of an operation where the accumulation and depletion of a substance are considered.
- 3) *Emission Factors*: Generic emission rates of pollutant release as a result of process activity or unit.
- 4) *Engineering Estimates*: Emission estimates using engineering principles and judgement surrounding chemical and physical processes at a facility type.

There are five emission source categories as outlined in IPCC (2006) that are applicable to methane: stationary fuel combustion, fugitive (flaring, venting, leakage), on-site transportation emissions, waste, and wastewater.

- 1) Stationary Fuel Combustion: Fuel is burned to produce useful heat or work (electricity, heat or steam) including boilers and internal combustion sources.
- 2) Fugitive: The sum of venting, flaring and leakage emissions.
 - a. Venting Controlled release of a process or waste gas to the atmosphere.
 - b. Flaring Controlled combustion of a gas or liquid stream not for the purpose of useful heat or work
 - c. Leakage Accidental releases and leaks of gases from fossil fuel processing, transmission and distribution
- On-Site Transportation: Gases released from transportation machinery used at an integrated facility. Examples include vehicles not licensed for use on public roads or above or below-ground mining operations.
- 4) Waste: Release of gases from waste disposal sources at the facility.
- 5) Wastewater. Fossil fuel-based emissions from wastewater and wastewater treatment.

Records must be kept for three years from the submission deadline. Submission of facility emissions can be completed online via the Single Window System (see Figures 30 and 31 for a reporting process overview, and ECCC (2023) for detailed guidance). The Single Window System allows the facility operator to input numerical values (tonnes) for each emission source and GHG, and the CO₂e will automatically be calculated.

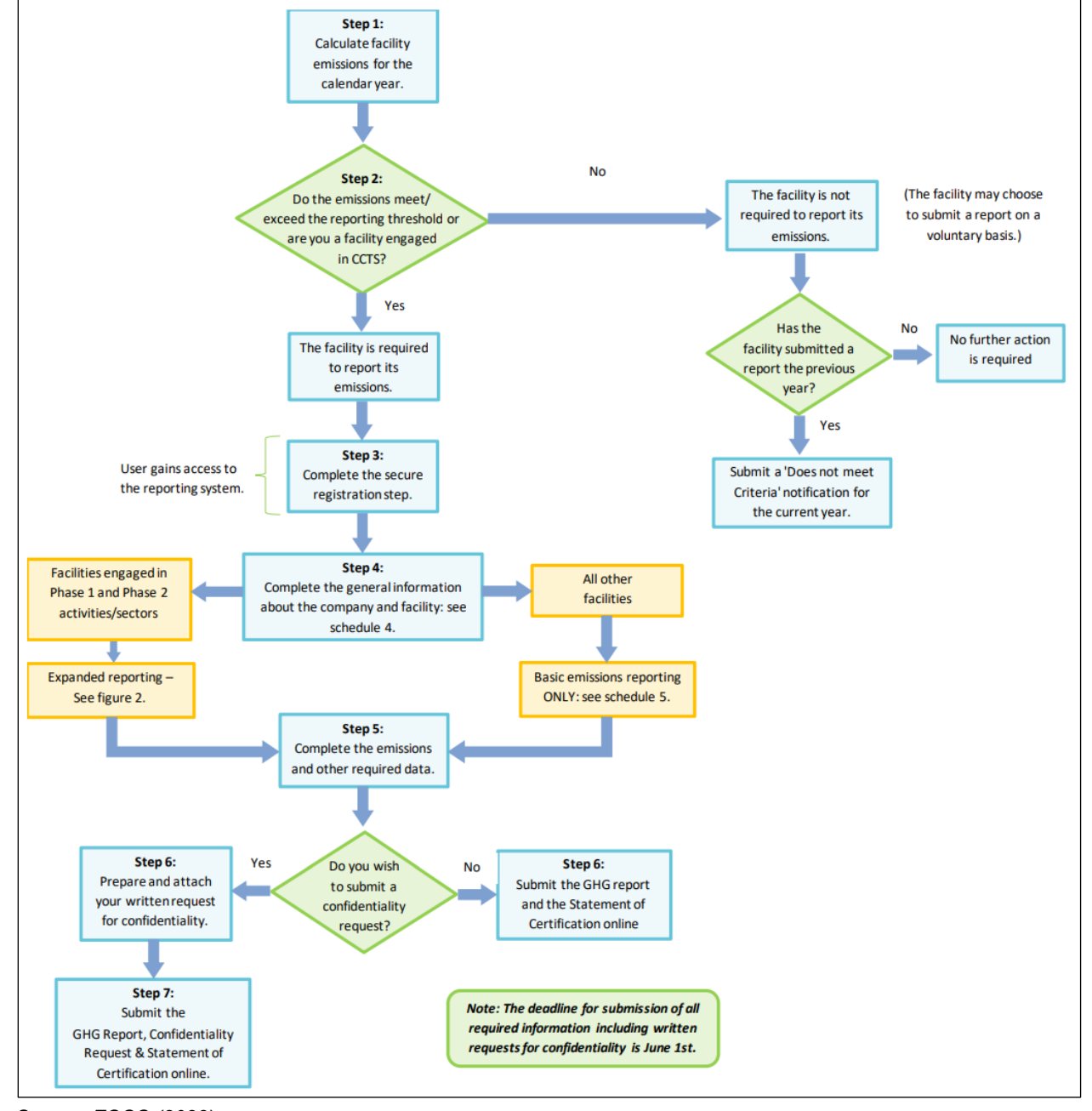


Figure 30. Reporting Process Overview

Source: ECCC (2023).

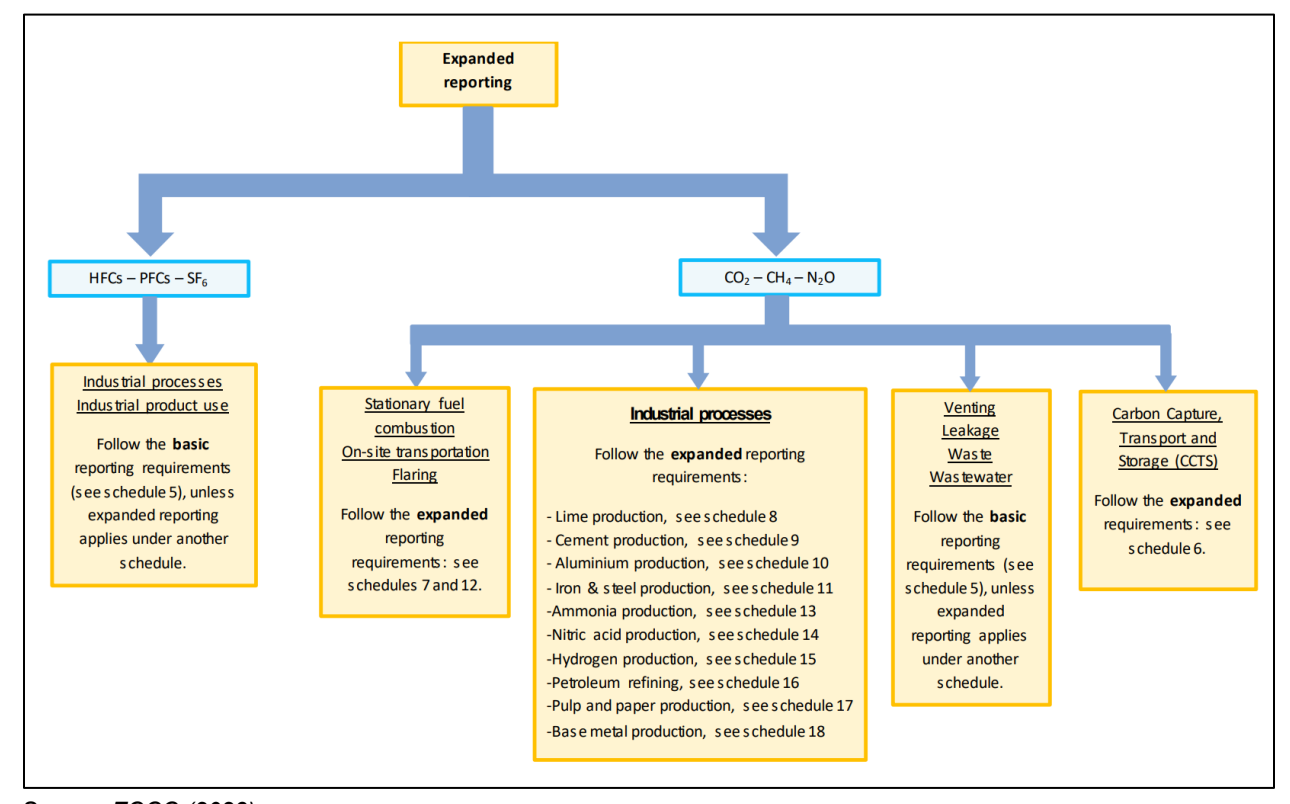


Figure 31. Expanded Reporting Overview

Source: ECCC (2023).

6.2 FEDERAL TAXATION BACKGROUND

In October 2016, ECCC (2016) published the *Pan-Canadian Framework on Clean Growth and Climate Change* which outlined an ambitious plan to cut total annual GHG emissions from 742 megatonnes (Mt) in December 2016 to 523 MT by 2030. To accomplish this objective, the federal government regards putting a price on carbon as the most effective means to drive innovation and energy efficiencies to reduce GHGs.

A schema for minimum national stringency pricing on carbon pollution is outlined in Schedule 4 of the *Greenhouse Gas Pollution Pricing Act* (Figure 32) (ECCC, 2018). Starting in 2018, pricing began at \$10 CAD/tonne CO₂e, and is planned to increase by \$15 per year to 2030 resulting in an end price of \$170 CAD/tonne CO₂e. Therefore, it is imperative that oil and gas operators do not overestimate or inaccurately report a facility's emissions as it will ultimately affect the operator's bottom line.

Figure 32. Carbon Pricing Per Year Per CO₂e Tonne

Calendar Year	Charge per CO ₂ e Tonne (\$)
2018	10
2019	20
2020	30
2021	40
2022	50
2023	65
2024	80
2025	95
2026	110
2027	125
2028	140
2029	155
2030	170

Note: Modified from ECCC. 2018.

A potential cap-and-trade system was proposed in July 2022 that allows federal regulators to issue a cap of emission for a registered facility with a flexible upper limit that requires verification. Facilities in this system would include liquefied natural gas (LNG) facilities and upstream oil and gas facilities, including offshore facilities. Operators could reduce emissions, purchase offset credits or contribute to a yet-to-be-established decarbonization fund – auctioning of allowances might be considered in later compliance periods. Discussions between industry and regulators are still ongoing, and if the system is approved it would be phased in between 2026-2030.

6.3 SUMMARY AND RECOMMENDATIONS

Based on the analysis herein, the most accurate method to observe and report methane data is through direct measurement based on available technology. From a federal regulatory perspective, a component leaking methane at or above 500 ppmv must be repaired and thus a concentration-based detection device is required to uphold this requirement. From a federal reporting and taxation perspective, a facility emitting 10,000 or more tonnes/year CO₂e must submit a report and adhere to any applicable carbon pollution pricing – thus a mass emission device with a high level of accuracy has clear benefits.

The alternate approach to direct measurement involving the use of average Emission Factor (EF), Screen Value Range (SVR) or Screening Value Correlation Equation (SVCE) methods sourced from EPA (1995) (and the later revised CAPCOA, 1999 unit-specific equations), is associated with a relatively high level of variability and uncertainty when compared with a direct measurement methodology. EPA (1995) acknowledges the deficiencies of the EF/SVR/SVCE methods that were intended to represent a broad estimate of emissions from a site-wide population of equipment. This can span "several orders of magnitude" and "are not necessarily an accurate indication of the mass emission rate from an individual piece of equipment." (US EPA, 1995).

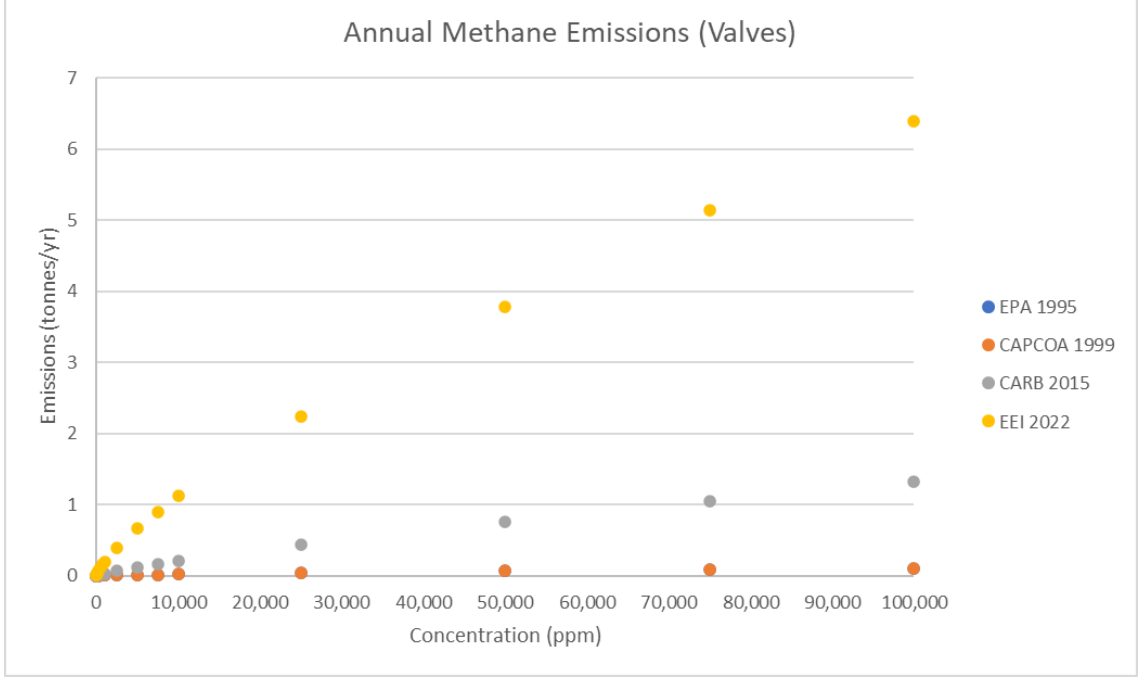
CARB (2015) later developed unit-specific correlations using approved Method 21 devices and a hi-flow sampler in an effort to better characterize the equations with a measurable methane quantity (kg/hr). When compared to the EPA (1995) and CAPCOA (1999) equations, the CARB (2015) resulted in at least an order of magnitude greater calculated emission rate.

Equilibrium completed a linear regression study in 2022 using a private dataset which resulted in a correlation equation with nearly two orders of magnitude greater difference compared to EPA (1995) equations for specifically valves (insufficient data was available to compare the remaining component categories). This may be due in part to the EPA (1995) equations being derived for VOC rather than specifically methane.

All four study's equations are compared for the 'Valves' component type in Figure 33 using generic concentration values from 10 ppm to 100,000 ppm and calculating the respective kg/hr, which in turn is converted to tonnes per year. The results demonstrate that when infrastructure-specific data are collected (simultaneous measurements of concentration and emission rates for CH4; EEI 2022 result in Figure 33), a multiple fold difference can result in the calculated GHG emission rate compared to the use of historical regression equations for VOC and natural gas emissions (e.g., US EPA, 1995; CAPCOA, 1999; CARB, 2015). Use of the historical equations would have underestimated mass emission rates for the particular dataset evaluated by EEI (2022), although leak detection capability would not be affected.

Annual Methane Emissions (Valves) 7

Figure 33. Calculated Methane Emissions for Valves Using Various Correlation Equations



Note: EPA (1995) datapoints are very similar to CAPCOA (1999) such that they are hidden at this scale. Tonnes/yr were calculated by using the kg/hr value from the respective study's equation for valves and multiplied by 8.76. Generic concentration values (ppm) were used to calculate kg/hr starting from 10 ppm to 100,000 ppm.

Several rationales could explain this multi-fold difference:

- unique climatic conditions and variables (temperature, wind);
- specific industrial process-related conditions (pressure, temperature of fluid stream);
- differences in operator equipment; and/or,
- differences in equipment calibration and testing technique.

This highlights the importance of generating facility or industrial-process specific regressions in order to achieve improved accuracy on the reporting of GHG emissions based on data collected from LDAR programs. Each facility is unique in number of component types, component sizes, pressures, and gas stream composition. Universal formulae applied to an entire industry will be associated with uncertainty and variability in reporting. It is unclear as to whether the EEI (2022) dataset is a conservative representation for the industry. Further work by industry may identify smaller regression slopes for predicted mass emission rates from ppmv concentrations, which in turn are used to determine GHG emission-related taxation.

Future studies would include collection of Method 21 concentration-based data simultaneously with mass emission rate data for regression development. Various Method 21 devices could be used, including OGI. Various mass emission rate detection devices could be employed. As the dataset of regressed CH₄ concentrations versus emission rates expands, larger patterns may be demonstrated allowing for critical variables to be identified and used to refine regressions to satisfy regulatory requirements of LDAR programs and GHG emissions reporting related to taxation rules. Data sharing would be of benefit to the entire industry and would expedite refinement of the process for improved efficiency and program implementation cost.

7 CLOSURE

Equilibrium Environmental Inc. has prepared this document for the exclusive use of Petroleum Technology Alliance Canada and Clean Resource Innovation Network solely for the purpose of assisting in the management of methane emissions. Any uses which a third party makes of this document, or any reliance on decisions made based on it, are the responsibility of such third parties. Equilibrium Environmental Inc. accepts no duty or care to any other person or any liability or responsibility whatsoever, for any losses, expenses, damages, fines, penalties, or other harm that may be suffered or incurred by any other person as a result of the use of, reliance on, any decision made, or any action taken based on this document. Nothing in this document is intended to constitute or provide a legal opinion.

The data review, analysis, and recommendations were limited to the data that has been collected to date, and the accuracy of the underlying dataset that was provided to Equilibrium cannot be verified and is not implied. Equilibrium Environmental Inc. believes information presented in this report is accurate but cannot guarantee or warrant its accuracy. If the database or applicable standards change, or additional information becomes available at a future time, modifications to the findings, conclusions, and recommendations in this document may be necessary. Any questions regarding this document should be directed to Anthony Knafla or Matthew Sommers at (403) 286-7706.

Sincerely,

Equilibrium Environmental Inc.

Matthew Sommers, M.Sc, P.Geo

Environmental Scientist

Report writing, literature review, data analysis

Anthony L. Knafla, M.Sc., P.Biol., DABT, QP

Founder/ Risk Assessment Specialist

Study design, senior guidance, report writing, report review

8 REFERENCES

Abdel-Moati, H., Morris, J., Zeng, Y., Kangas, P., and McGregor, D. 2015. New Optical Gas Imaging Technology for Quantifying Fugitive Emission Rates. International Petroleum Technology Conference, IPTC-18471-MS, pp. 1-6.

Alden, C.B., Coburn, S.C., Wright, R.J., Baumann, E., Cossel, K., Perez, E., Hoenig, E., Prasad, K., Coddington, I., and Rieker, G.B. 2019. Single-Blind Quantification of Natural Gas Leaks from 1 km Distance Using Frequency Combs. Environmental Science & Technology, vol. 59, pp. 2908-2917.

Aldhafeeri, T., Tran, M-K., Vrolyk, R., Pope, M. and M Fowler. A review of methane gas detection sensors: recent developments and future perspectives. Inventions 2020, 5(3), 28. https://doi.org/10.3390/inventions5030028

Barton-Grimley, R.A., Bhrir, A.R., Kooi, S.A., Collins, J.E., Harper, D.B., Notari, A., Lee, J., DiGangi, J.P., Choi, Y., and Davis, K.J. 2022. Evaluation of the High Altitude Lidar Observatory Methane Retrievals During the Summer 2019 ACT-America Campaign. Atmospheric Measurement Techniques. Open Access Pre-Print Discussion, pp. 1-42.

Bell, C., Rutherford, J., Brandt, A., Sherwin, E., Vaughn, T., and Zimmerle, D. 2022. Single-blind determination of methane detection limints and quantification accuracy using aircraft-based LiDAR. Elementa: Science of the Anthropocene, vol. 10, no. 1, pp. 1-12.

Brandt, A.R., Geath, G.A., and Cooley, D. 2016. Methane Leaks from Natural Gas Systems Follow Extreme Distributions. Environmental Science & Technology. Vol. 50, pp. 12512-12520. DOI: 10.1021/acs.est.6b04303

Bridger Photonics Inc. 2023. 5 Questions to Ask When Evaluating Methane Emissions Detection Technologies. Accessed July 2023. https://www.bridgerphotonics.com/blog/5-questions-ask-when-evaluating-methane-emissions-detection-technologies

California Air Pollution Control Officers Association (CAPCOA). 1999. California Implementation Guidelines for Estimating Mass Emissions of Fugitive Hydrocarbon Leaks at Petroleum Facilities. pp 1-44.

Cheadle. LC., Tran, T., Nyarady, J.F., and Lozo, C. 2022. Leak detection and repair data from California's oil and gas methane regulation show decrease in leaks over two years. Environmental Challenges, vol. 8, pp. 1-8.

Coblenz Society. 2018. Methane *in*: National Institute of Standards and Technology U.S. Department of Commerce, NIST Chemistry WebBook, SRDS 69. Accessed June 2023. https://webbook.nist.gov/cgi/cbook.cgi?Name=Methane&Units=SI

Concawe, 2017. Air pollutant emission estimation methods for E-PRTR reporting by refineries. 2017 edition. Report no. 4/17. ISBN 978-2-87567-070-0. Brussels.

Concawe, 2015. Techniques for detecting and quantifying fugitive emissions – results of comparative field studies. 2015 edition. Report no. 6/15. ISBN 978-2-87567-049-6. Brussels.

Connolly, J.J., Robinson, R.A., and Gardiner, T.D. 2019. Assessment of the Bacharach Hi Flow® Sampler characteristics and potential failure modes when measuring methane emissions. Measurement, vol. 145, pp. 226-233.

Environment and Climate Change Canada (ECCC). 1999. Canadian Environmental Protection Act. https://laws-lois.justice.gc.ca/PDF/C-15.31.pdf

Environment and Climate Change Canada (ECCC). 2016. Pan-Canadian Framework on Clean Growth and Climate Change. https://publications.gc.ca/collections/collection_2017/eccc/En4-294-2016-eng.pdf

Environment and Climate Change Canada (ECCC). 2018a. Regulations Respecting Reduction in the Release of Methane and Certain Volatile Organic Compounds (Upstream Oil and Gas Sector). Extra Vol. 152, No.1. Canadiana Gazette. Part II. SOR/2018-66 April 4, 2018.

Environment and Climate Change Canada (ECCC). 2018b. Greenhouse Gas Pollution Pricing Act. Enacted June 21, 2018, last amended July 1, 2023. https://laws-lois.justice.gc.ca/PDF/G-11.55.pdf

Environment and Climate Change Canada (ECCC). 2019. SOR-2018-66: Guidance Document on the Regulations Respecting Reduction in the Release of Methane and Certain Volatile Organic Compounds (Upstream Oil and Gas Sector), pp. 1 – 29.

Environment and Climate Change Canada (ECCC). 2021. Review of Canada's methane regulations for the upstream oil and gas sector. Her Majesty the Queen in Right of Canada, Minister of Environment and Climate Change, December 2021. EC21214. https://www.canada.ca/en/environment-climate-change/services/canadian-environmental-protection-act-registry/review-methane-regulations-upstream-oil-gas-sector.html

Environment and Climate Change Canada (ECCC). 2023a. National Inventory Report 1990-2021: Greenhouse Gas Sources and Sinks in Canada. Cat. No. En81-4E-PDF, ISSN: 1910-7064, pp. 1-268.

Environment and Climate Change Canada (ECCC). 2023b. Technical Guidance on Reporting Greenhouse Gas Emissions. https://publications.gc.ca/collections/collection-2023/eccc/En81-29-2023-eng.pdf

Harvey, D. 2021. Chapter 14 - Mass spectrometric detectors for gas chromatography *in*: Gas Chromatography, Poole, C.F. pp. 399-424.

Hetek Solutions Inc. (Hetek). 2023. Hetek Flow Sampler User Manual, version 1.6 – April 2023, Document #6.11.

Highwood Emissions Management. 2022. How much Gas is that?!. https://highwoodemissions.com/tools/how-much-gas-is-that/

IEA, 2023. Global Methane Tracker 2023. IEA, Paris, License: CC BY 4.0. https://www.iea.org/reports/global-methane-tracker-2023

Innocenti, F., Robinson, R., Gardiner, T., Finlayson, A., and Connor, A.J.R.S. 2017. Differential absorption lidar (DIAL) measurements of landfill methane emissions. Remote Sensing. Vol. 9, No. 9, pp. 1-11.

Intergovernmental Panel on Climate Change (IPCC). 2013. Climate Change 2013: The Physical Science Basis. Contribution of Working Group I to the Fifth Assessment Report of the Intergovernmental Panel on Climate Change. Cambridge University Press, Cambridge, United Kingdom and New York, NY, USA.

Intero – The Sniffers (Intero). 2023. Reporting methane venting emissions: why you should step away from modeling and use a measurement-based approach. Accessed June 2023. https://www.the-sniffers.com/news/reporting-methane-venting-emissions-why-you-should-step-away-from-modeling-and-use-a-measurement-based-approach/

Jamin, Y. 2018. Update of Equipment, Component and Fugitive Emissions Factors for Alberta Upstream Oil and Gas, pp. 1-95.

Kang, R., Liatsis, P., and Kyritsis, D.C. 2022. Emission Quantification via Passive Infrared Optical Gas Imaging: A Review. Energies, Vol. 15, No. 3303, pp. 1-32.

Ke, J., Li, S., and Zhao, D. The application of leak detection and repair program in VOCs control in China's petroleum refineries. Air & Waste Management Association. Vol. 70, No. 4, pp. 862-875.

LongPath Technologies (LongPath). 2023. LongPath's Technology. Accessed June 2023. https://www.longpathtech.com/technology

Mendes, L.B., Ogink, N.W.M., Edouard, N., Van Dooren, H.J.C., Tinoco, I.D., and Mosquera, J. 2015. NDIR Gas Sensor for Spatial Monitoring of Carbon Dioxide Concentrations in Naturally Ventilated Livestock Buildings. Sensors, Vol. 5, No. 5, pp. 11239-11257.

Minister of Justice, 2022. SOR/2020-231: Reduction in the Release of Volatile Organic Compounds Regulations (Petroleum Sector), Schedule 3, pp. 49. SOR-2020-231.pdf (justice.gc.ca)

Mitchell., A.L., Tkacik, D.S., Roscioli, J.R., Herndon, S.C., Yacovitch, T.I., Martinez, D.M., Vaughn, T.L., Williams, L.L., Sullivan, M.R., Floerchinger, C., Omara, M., Subramanian, R., Zimmerle, D., Marchese, A.J., and Robinson, A.L. 20155. Measurements of Methane Emission from Natural Gas Gathering Facilities and Processing Plants: Measurement Results. Environmental Science & Technology. Vol. 49, No. 5, pp. 3219-3227.

Nanoplus. (2023). Tunable Diode Laser Absorption Spectroscopy. Accessed June, 2023. https://nanoplus.com/applications/tunable-diode-laser-absorption-spectroscopy

Opgal Optronic Industries Ltd. (Opgal). 2022. Advancements In Bottom-Up Quantification Of Fugitive Emissions Using Optical Gas Imaging. Accessed June, 2023. https://www.opgal.com/blog/optical-gas-imaging-ogi/advancements-in-bottom-up-quantification-of-fugitive-emissions-using-optical-gas-imaging/

Providence Photonics, LLC (Providence). 2018. Quantitative Optical Gas Imaging QL320 Training. v.1.0.0.7. Accessed June 2023. https://dcmarketplace.nyc3.digitaloceanspaces.com/dcconference/2018/trainingmaterial/Advanced%20topics%20in%20Quantitative%20Optical%20Gas%20Imaging.pdf

RAE Systems (RAE). *In press*. RAE Systems PID Training Outline. Application Note AP-000, 04/05/CW. https://sps.honeywell.com/content/dam/his-sandbox/products/gas-and-flame-detection/documents/Application-Note-000 RAE-Systems-PID-Training-Outline 04-05.pdf

RAE Systems (RAE). 2014. The PID Handbook: Theory and Applications of Direct-Reading Photoionization Detectors. Honeywell, ISBN 0692026622.

Ravikumar, A.P., Singh, D., Barlow, B., Robison, C., and Funk, W. 2020. Alberta Methane Field Challenge Final Report. https://static1.squarespace.com/static/625ef017027b5d0e69e4b7f2/t/62bb550ec4ebb92ac649b 0c1/1656444176962/AMFC FinalReport v6.pdf

Sage ATC Environmental Consulting LLC (Sage). 2019. Air Resources Board IFB No. 13-434: Enhanced Inspection & Maintenance for GHG & VOCs at Upstream Facilities – (Revised), pp. 1-289.

Sizemore, S. 2023. LongPath Tech gas field. National Institute of Standards and Technology. Accessed July 2023. https://www.nist.gov/image/gasfieldpng

Taylor, C.D., Chilton, J.E., and Martikainen, A.L. 2008. Use of infrared sensors for monitoring methane in underground mines. Center for Disease Control and Prevention, National Institute for

Occupational Safety and Health, Pittsburgh, Pennsylvania, USA. https://www.cdc.gov/niosh/mining%5C/UserFiles/works/pdfs/uoisf.pdf

Teledyne FLIR LLC (FLIR). 2020. The Latest Technology for Quantifying Gas Leaks. Accessed June, 2023. https://www.flir.ca/discover/webinars/ogi-webinars/the-latest-technology-for-quantifying-gas-leaks/

Teledyne FLIR LLC (FLIR). 2023. The Science Behind Optical Gas Imaging. Accessed June, 2023. https://www.flir.ca/discover/instruments/gas-detection/the-science-behind-optical-gas-imaging/

United States Environmental Protection Agency, 1995. 1995 Protocol for Equipment Leak Emission Estimates. Emission Standards Division. Office of Air and Radiation, Office of Air Quality Planning and Standards, Research Triangle Park, North Carolina 27711. November 1995. EPA-453/R-95-017.

United States Environmental Protection Agency (EPA). 2008. Alternative Work Practice To Detect leaks From Equipment. Document No. E8-30196, pp. 78199-78219.

United States Environmental Protection Agency (EPA). 2011. EPA Handbook: Optical and Remote Sensing for Measurement and Monitoring of Emissions Flux of Gases and Particulate Matter. Doc. No. EPA 454/B-18-008, pp. 1-346.

United States Environmental Protection Agency (EPA). 2016. Greenhouse Gas Reporting Rule: Leak Detection Methodology Revisions and Confidentiality Determinations for Petroleum and Natural Gas Systems. Document No. EPA-HQ-OAR-2015-0764. https://www.govinfo.gov/content/pkg/FR-2016-11-30/pdf/2016-27981.pdf

United States Environmental Protection Agency (EPA). 2017. Method 21 – Volatile Organic Compound Leaks, pp. 1 – 7. https://www.epa.gov/sites/default/files/2017-08/documents/method 21.pdf

Wang, Z., Kamimoto, T., and Deguchi, Y. 2018. Industrial Applications of Tunable Diode Laser Absorption Spectroscopy, *in*: Temperature Sensing, edited by Stanimiovic, I. and Stanimirovic, Z. DOI: 10.5772/intechopen.77027.

Wiedmann, D., Hirst, B., Jones, Jones, M., Ijzermans, R., Randell, D., Macleod, N., Kannath, A., Chu, J., and Dean, M. 2022. Locating and quantifying methane emissions by inverse analysis of path-integrated concentration data using a Markov-Chain Monte Carlo approach. ACS Earth Space Chem, 6, 9: 2190-2198. https://pubs.acs.org/doi/10.1021/acsearthspacechem.2c00093

Wikipedia. (2023). Tunable diode laser absorption spectroscopy. Accessed June 2023. https://en.wikipedia.org/wiki/Tunable diode laser absorption spectroscopy#Basic principles

Yakovlev, S.V. Sadovnikov, S.A, and Romanovskii, O.A. 2022. Mobile Airborne Lidar for Remote Methane Monitoring: Design, Simulation of Atmospheric Measurements and First Flight Tests. Remote Sensing, Vol. 14, No. 24, pp. 1-24.

Zavala-Araiza, D., Herndon, S.C., Roscioli, J.R., Yacovitch, T.I., Johnson, M.R., Tyner, D.R., Omara, M., and Knighton, B. 2018 Methane Emissions from Oil and /gas /production Sites in Alberta, Canada. Elementa Science of the Anthropocene, vol. 6: 27, pp. 1 – 10.

Zeng, Y., Morris, J., Sanders, A., Mutyala, S., and Zeng, C. 2017. Methods to determine response factors for infrared gas imagers used as quantitative measurement devices. Journal of the Air & Waste Management Association, Vol. 67, No. 11, pp. 1180-1191. https://doi.org/10.1080/10962247.2018.1540366

Zeng, Y. and J. Morris. 2019. Detection limits of optical gas imagers as a function of temperature differential and distance. Journal of the Air & Waste Management Association. 69(3), 351-361.

Zhao, G. Wu, X. Zhu, S., Mei, L., and Svanberg, S. 2013. Method to Monitor Atmospheric Mercury by a Differential Absorption Lidar System. Asia Communication and Photonics Conference 2013. OSA Technical Digest, paper AF4H.5.